Cell Reports

Article

Identification of a population of peripheral sensory neurons that regulates blood pressure

Graphical abstract

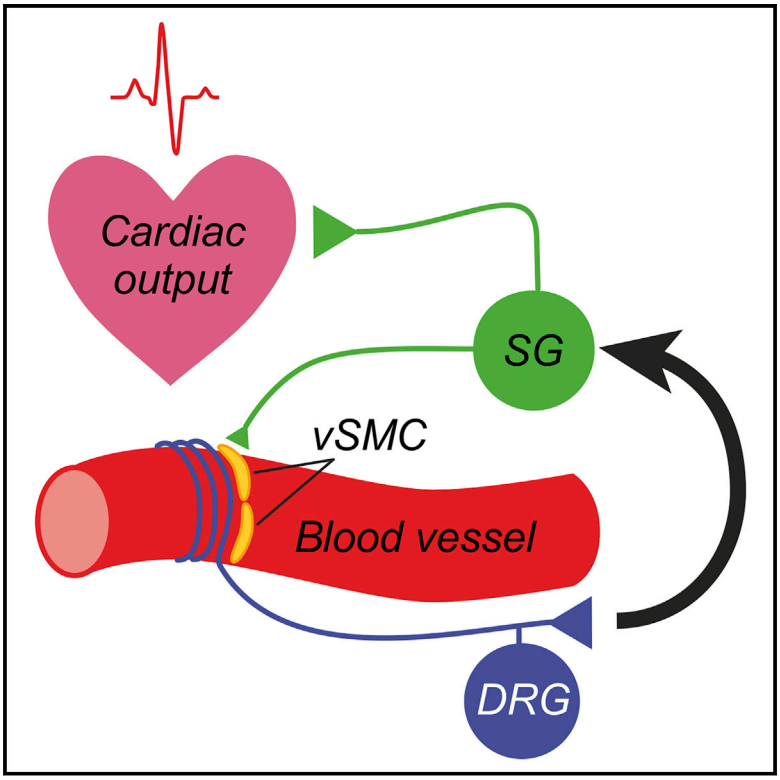

Authors

Chiara Morelli, Laura Castaldi, Sam J. Brown, ..., Stefan G. Lechner, Robert Prevedel, Paul A. Heppenstall

Correspondence

paul.heppenstall@sissa.it

In brief

Morelli et al. identify a subpopulation of peripheral sensory neurons marked by TrkC and Th that projects to distal blood vessels. They demonstrate that these neurons regulate peripheral perfusion, blood pressure, and heart rate.

Highlights

- TrkC$^+$/Th$^+$ DRG neurons project to blood vessels
- Local stimulation of TrkC$^+$ DRG neurons decreases vessel diameter and blood flow
- Systemic activation of TrkC$^+$ DRG neurons increases blood pressure and heart rate
- Ablation of TrkC$^+$ neurons dysregulates cardiovascular homeostasis and is lethal

Morelli et al., 2021, Cell Reports *35*, 109191
June 1, 2021
https://doi.org/10.1016/j.celrep.2021.109191

CellPress

Cell Reports

CellPress
OPEN ACCESS

Article

Identification of a population of peripheral sensory neurons that regulates blood pressure

Chiara Morelli,[1,2,3,10] Laura Castaldi,[1,2,10] Sam J. Brown,[1] Lina L. Streich,[3,5] Alexander Websdale,[1] Francisco J. Taberner,[1,4] Blanka Cerreti,[1] Alessandro Barenghi,[1,9] Kevin M. Blum,[6,7] Julie Sawitzke,[1] Tessa Frank,[1] Laura K. Steffens,[5] Balint Doleschall,[1] Joana Serrao,[1,9] Denise Ferrarini,[1,9] Stefan G. Lechner,[4] Robert Prevedel,[1,5,8] and Paul A. Heppenstall[1,2,9,11,*]

[1]EMBL Rome, Via Ramarini 32, Monterotondo 00015, Italy
[2]Molecular Medicine Partnership Unit (MMPU), Heidelberg, Germany
[3]Collaboration for joint PhD degree between EMBL Heidelberg, Heidelberg, Germany, and Heidelberg University, Faculty of Biosciences, Heidelberg, Germany
[4]Institute of Pharmacology, Heidelberg University, Im Neuenheimer Feld 366, 69120 Heidelberg, Germany
[5]Cell Biology and Biophysics Unit, European Molecular Biology Laboratory (EMBL), Heidelberg, Germany
[6]Center for Regenerative Medicine, the Abigail Wexner Research Institute at Nationwide Children's Hospital, Columbus, OH, USA
[7]Department of Biomedical Engineering, the Ohio State University, Columbus, OH, USA
[8]Developmental Biology Unit, European Molecular Biology Laboratory (EMBL), Heidelberg, Germany
[9]Present address: Scuola Internazionale Superiore di Studi Avanzati, Via Bonomea, 265, 34136 Trieste, Italy
[10]These authors contributed equally
[11]Lead contact
*Correspondence: paul.heppenstall@sissa.it
https://doi.org/10.1016/j.celrep.2021.109191

SUMMARY

The vasculature is innervated by a network of peripheral afferents that sense and regulate blood flow. Here, we describe a system of non-peptidergic sensory neurons with cell bodies in the spinal ganglia that regulate vascular tone in the distal arteries. We identify a population of mechanosensitive neurons, marked by tropomyosin receptor kinase C (TrkC) and tyrosine hydroxylase in the dorsal root ganglia, which projects to blood vessels. Local stimulation of TrkC neurons decreases vessel diameter and blood flow, whereas systemic activation increases systolic blood pressure and heart rate variability via the sympathetic nervous system. Ablation of the neurons provokes variability in local blood flow, leading to a reduction in systolic blood pressure, increased heart rate variability, and ultimately lethality within 48 h. Thus, a population of TrkC$^+$ sensory neurons forms part of a sensory-feedback mechanism that maintains cardiovascular homeostasis through the autonomic nervous system.

INTRODUCTION

Regulation of blood pressure through control of blood flow and cardiac output is essential for tissue and organ homeostasis. This is achieved through local mechanisms intrinsic to blood vessels, such as endothelial-cell-derived signaling, and via neuronal mechanisms that regulate cardiovascular function at a global level to coordinate vascular resistance and modulate cardiac output (Thomas, 2011; Westcott and Segal, 2013). Indeed, major blood vessels are surrounded by a dense plexus of nerves made up of post-ganglionic sympathetic efferent axons and sensory axons from the spinal ganglia. These exert broadly opposing effects on vascular resistance, such that activation of sympathetic neurons causes vasoconstriction, whereas activity in sensory nerves produces vasodilation.

Two types of perivascular sensory neuron have been described previously: peptidergic vascular afferents, which originate in the dorsal root ganglia (DRGs), and mechanosensitive baroreceptors of the nodose and petrosal ganglia (Coleridge and Coleridge, 1980; Westcott and Segal, 2013). Peptidergic sensory neurons can be identified by their expression of neuropeptides, such as substance P (SP) and calcitonin gene-related peptide (CGRP), and the ion channel TRPV1 (Gibbins et al., 1985; Vass et al., 2004). They are activated by mechanical, chemical, and thermal stimuli (Adelson et al., 1997; Bessou and Perl, 1966; Haupt et al., 1983) and project to vascular beds throughout the body (Burnstock and Ralevic, 1994). As well as having an afferent sensory function, it has long been appreciated that these neurons also perform an effector role through local axon reflexes (Bayliss, 1901; Bruce, 1913). Thus, their activation by noxious stimuli in tissue can provoke a potent vasodilator effect through the release of CGRP and purines (Burnstock, 2007; Kawasaki et al., 1988), as well as plasma extravasation through SP (Lembeck and Holzer, 1979).

Baroreceptors are stretch-sensitive sensory neurons that project from the cervical ganglia to the aorta and carotid sinuses (Kirchheim, 1976). Their endings are embedded in artery walls, and they continuously monitor arterial blood pressure through

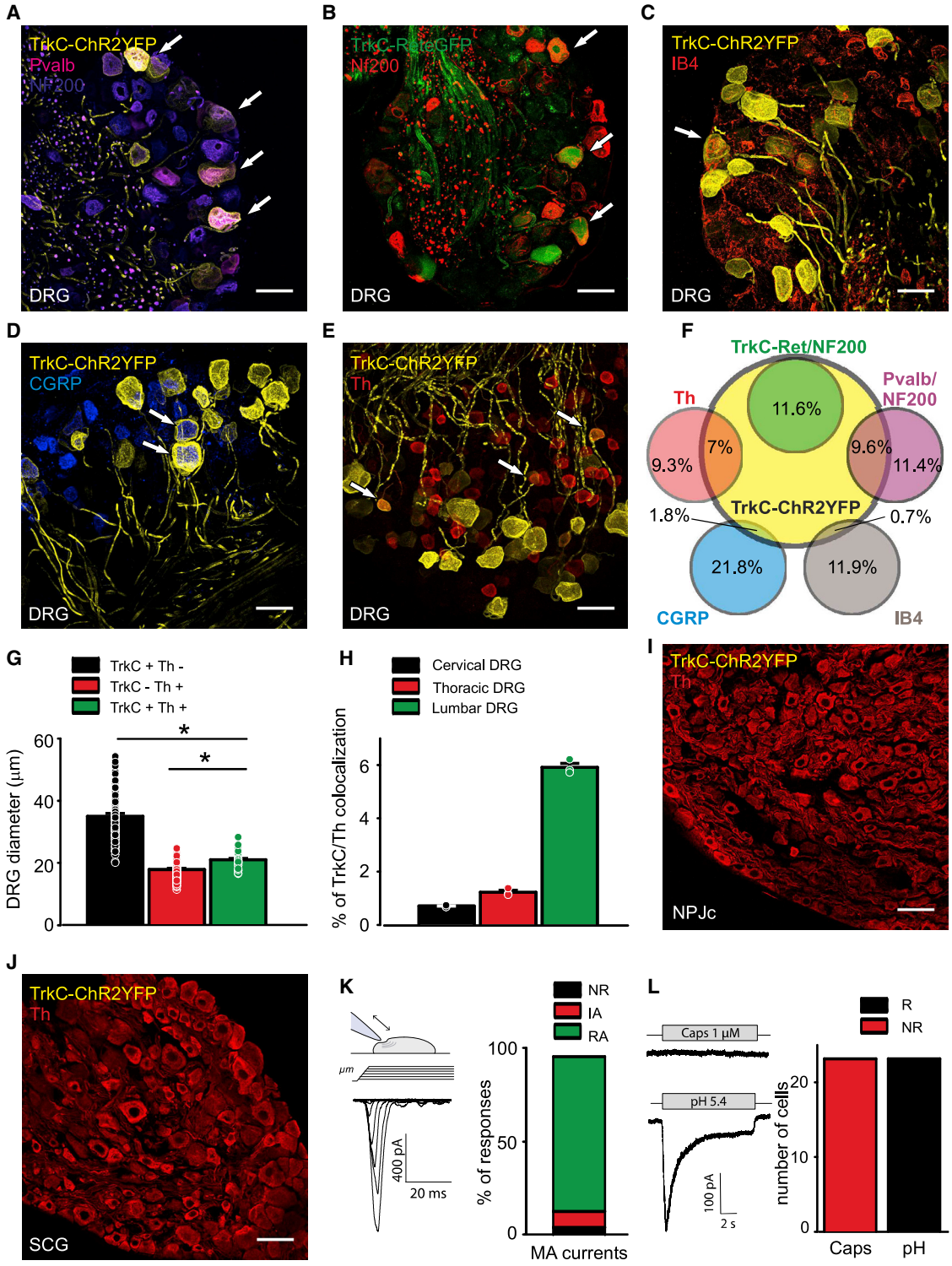

Figure 1. TrkC expression in peripheral ganglia

(A–F) Immunofluorescent staining of DRG sections from TrkC^{CreERT2}::Rosa26$^{ChR2\text{-}YFP}$ (yellow) showed that 9.6% of DRG neurons co-express markers of proprioceptors (Pvalb, red; NF200, magenta) (A and F) and 11.6% of slowly adapting (SA) field mechanoreceptors (Ret, green; NF200, red) (B and F). Very few TrkC^{+} neurons overlap with markers of non-peptidergic nociceptors (IB4, red) (C and F) or peptidergic nociceptors (CGRP, blue) (D and F); 7% of all DRG neurons are also positive for Th (red), a marker of C-fiber low-threshold mechanoreceptors (C-LTMRs) (E and F). (F) Quantification of TrkC co-expression with the other markers in DRGs showing the percentage of total neurons.

(legend continued on next page)

the mechanosensitive ion channels Piezo1 and Piezo2 (Zeng et al., 2018). They are exquisitely sensitive to distension of the vessel wall, such that their firing rate fluctuates as arterial pressure changes through the cardiac cycle. They function to minimize short-term fluctuations in blood pressure; thus, increases in baroreceptor activity provoke arteriolar vasodilation through inhibition of the sympathetic nervous system and reduction in cardiac output via decreased sympathetic and increased parasympathetic input. Conversely, decreased baroreceptor activity produces vasoconstriction and increased cardiac output (Wehrwein and Joyner, 2013). Both clinical and experimental studies have demonstrated that a reduction in baroreceptor function results in a marked increase in the lability of blood pressure and heart rate (Heusser et al., 2005; Ito and Scher, 1981; Robertson et al., 1993; Rodrigues et al., 2011; Sved et al., 1997).

Beyond peptidergic vascular afferents and baroreceptors, further classes of perivascular sensory neurons are likely to exist, especially those involved in sensing vessel wall stretch. However, their identification has been hampered by their inaccessibility to classical neurophysiological methods and by a paucity of molecular markers by which to distinguish them. Here, we identify a population of non-peptidergic DRG neurons that coexpress tropomyosin receptor kinase C (TrkC) and tyrosine hydroxylase and project to distal arteries. We demonstrate that experimental ablation of these neurons leads to dysregulation of blood flow and heart rate, decreased blood pressure, and ultimately death of mice within 48 h. Moreover, their optogenetic or chemogenetic activation provokes vasoconstriction, marked increases in blood pressure, and heart rate variability, which are dependent upon activation of the sympathetic nervous system and pain behavior. Thus, we describe a population of vascular sensory afferents that, together with peptidergic afferents and baroreceptors, coordinate vascular resistance and cardiac output.

RESULTS

To characterize subpopulations of peripheral neuron, we generated an inducible TrkC^{CreERT2} mouse line and crossed it with a Rosa26$^{ChR2\text{-}YFP}$ reporter line to examine the co-localization of TrkC with established cellular markers in adult peripheral ganglia. We first investigated the DRG, where TrkC has previously been shown to colocalize with parvalbumin (Pvalb; a marker of proprioceptors [Copray et al., 1994]), and Ret (as a marker of the Aβ field mechanoreceptors [Bai et al., 2015]); 31% of all DRG neurons were positive for TrkC^{CreERT2}-driven yellow fluorescent protein (YFP). Of these, 31% of TrkC^{+} neurons were labeled with Pvalb and NF200 (Figures 1A and 1F; 9.6% of all DRG neurons) and 38% co-expressed Ret and NF200 (Figures 1B and 1F; 11.6% of all DRG neurons), whereas 31% of TrkC^{+} neurons expressed neither those markers nor NF200 (Figures 1F; 9.5% of all DRG neurons). To identify that third population, we stained DRG sections for markers of non-peptidergic nociceptors (IB4), peptidergic nociceptors (CGRP), and C-fiber low-threshold mechanoreceptors (C-LTMRs and tyrosine hydroxylase [Th] [Li et al., 2011]). We observed minimal overlap between TrkC^{CreERT2}-driven YFP and IB4 (Figures 1C and 1F) and CGRP (Figures 1D and 1F) but found that most TrkC^{+}/NF200^{-} neurons expressed Th (Figures 1E and 1F). TrkC^{+}/Th^{+} neurons were significantly smaller than TrkC^{+}/Th^{-} neurons (Figure 1G); they were also more prevalent in lumbar DRG than thoracic or cervical DRG (Figures 1H and S1A–S1C). We further investigated whether TrkC^{+}/Th^{+} neurons were evident in other peripheral ganglia. We observed robust Th labeling in the nodose-petrosal-jugular ganglion complex but no TrkC^{CreERT2}-mediated recombination (Figures 1I, S1D, and S1E). Similarly, sympathetic neurons in the paravertebral ganglia were positive for Th but negative for TrkC^{CreERT2} (Figures 1J, S1F, and S1G).

We next explored the response properties of isolated small TrkC^{+} DRG neurons using a whole-cell patch clamp. All neurons were responsive to mechanical stimulation, and most displayed a rapidly inactivating current indicative of Piezo2 activation (Figure 1K). Neurons were also activated by low pH but were not sensitive to the TRPV1 agonist capsaicin (Figures 1L and S1H–S1K). Action potentials had a short duration without a hump upon repolarization (Figures S1L and S1M), indicating that the neurons shared some electrophysiological properties with previously described Th^{+} neurons (Delfini et al., 2013). We further analyzed published single-cell RNA sequencing (RNA-seq) data of DRG neurons (Zeisel et al., 2018) and, consistent with our findings, distinguished a population of TrkC^{+}/Th^{+} neurons (46% of all TrkC neurons; 65% of all Th neurons) that expressed high levels of Piezo2 and the acid-sensing ion channel ASIC2 but were negative for parvalbumin, TRPV1, and CGRP (Figure S1N).

Given that Th^{+} C-LTMRs project to the skin and form longitudinal lanceolate endings around hair follicles (Li et al., 2011), we examined whole-mount preparations of skin for TrkC^{CreERT2}-driven YFP fluorescence. Although we observed clusters of TrkC^{+} Aβ field mechanoreceptors (Figure 2A), we were unable to detect any longitudinal lanceolate endings indicative of C-LTMRs. We did, however, discern TrkC^{+} cells surrounding arteries and arterioles (Figure 2A) throughout the body (Figures 2B–2D), which were positive for desmin, suggesting they may be vascular smooth muscle cells (vSMCs) (Figure 2E). Further characterization using an antibody against the vSMC marker

(G) TrkC^{+}/Th^{+} DRG neurons are significantly larger than TrkC^{-}/Th^{+} neurons and smaller than TrkC^{+}/Th^{-} neurons (298 neurons from three mice). *$p < 0.001$.
(H) Quantification of the number of DRG neurons co-expressing TrkC and Th at different spinal segmental levels, expressed as the percentage of the total number of DRG neurons (n = 3).
(I and J) TrkC is not expressed in the nodose-petrosal-jugular ganglion complex (I) and is not expressed in the superior cervical ganglion (J).
(K) Left, sketch depicting the mechanical-stimulation protocol and an example trace of a mechanically activated current (MA current) in a small TrkC^{+} neuron. Right, distribution of the different types of MA currents in the small TrkC^{+} neurons (24 neurons from three mice): rapidly adapting (RA), intermediate adapting (IA), and non-responding (NR).
(L) Left, example responses to capsaicin and pH 5.4 in a small TrkC^{+} neuron. Right, number of neurons responding (R) and non-responding (NR) to capsaicin or pH in small TrkC^{+} neurons. Arrows indicate co-expression of TrkC^{+} neurons with the other markers. Scale bars, 50 μm.

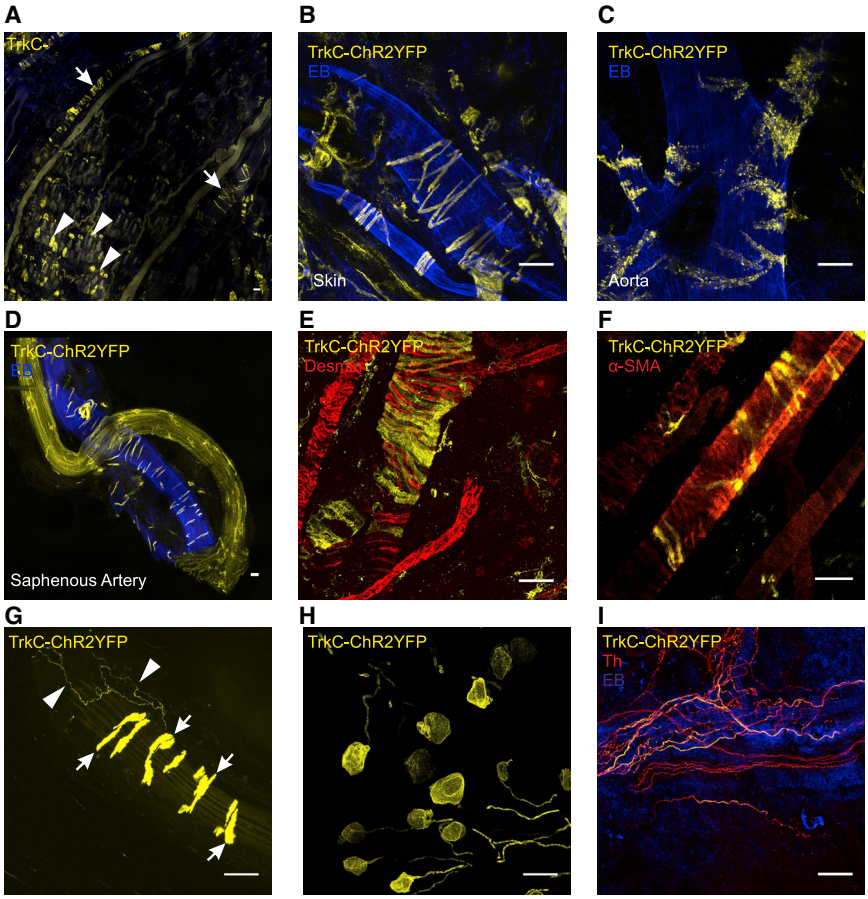

Figure 2. TrkC mediated recombination in peripheral tissue

(A–D) A whole-mount skin preparation from a $TrkC^{CreERT2}$::$Rosa26^{ChR2\text{-}YFP}$ mouse shows $TrkC^+$ Aβ field mechanoreceptors (arrowheads) and $TrkC^+$ cells surrounding blood vessels (arrows). (B–D) TrkC is expressed in perivascular cells throughout the body: skin (B), aorta (C), and saphenous artery (D). Mice were injected with Evans blue (EB) i.v. to visualize blood vessels; the saphenous nerve is also evident in (D).

(E) Immunohistochemical analysis with anti-desmin antibodies in $TrkC^{CreERT2}$::$Rosa^{26ChR2\text{-}YFP}$ mice reveals that TrkC marks a population of desmin-positive perivascular cells.

(F) Immunostaining with anti-α-SMA antibodies indicates that $TrkC^+$ cells are a subpopulation of vSMC.

(G) The vasculature is innervated by $TrkC^+$ neurons (arrowheads). $TrkC^+$ perivascular cells are also indicated (arrows).

(H and I) Intrathecal injection of 45 ng of 4-hydroxytamoxifen in $TrkC^{CreERT2}$::$Rosa26^{ChR2\text{-}YFP}$ mice leads to robust expression of YFP in DRGs (H) and in neurons innervating blood vessels (I) but not in $TrkC^+$ vSMC (I). $TrkC^+$ neurons innervating the vessels co-express the marker Th (I). Scale bars, 50 μm.

alpha smooth muscle actin (α-SMA) revealed that a subset of vSMCs were indeed $TrkC^+$ (Figure 2F).

Intriguingly, upon examination of vessels at higher magnification, it became evident that they were innervated by $TrkC^+$ neurons (Figure 2G). To visualize these afferents in the absence of contaminating YFP fluorescence from $TrkC^+$ vSMC, we injected the active tamoxifen metabolite 4-hydroxytamoxifen at low doses intrathecally into $TrkC^{CreERT2}$ mice to induce Cre expression only in DRGs (Figures S2A–S2L). After a single intrathecal (i.t.) 45-ng injection of 4-hydroxytamoxifen, we observed a robust recombination in DRGs (Figures 2H and S2A–S2F) and clearly visible innervation of the vessels (Figures 2I and S2G–S2L). Co-staining with Th revealed that all $TrkC^+$-vessel-innervating afferents were Th^+ and that they were interwoven with presumably sympathetic neurons, forming a dense plexus around vessels (Figure 2I). Such $TrkC^+$ innervation was observed primarily in the extremities of mice and not detected in the heart (Figure S3).

To explore the function of $TrkC^+$ neurons, we first took a loss-of-function approach using $TrkC^{CreERT2}$::$Avil^{iDTR}$ mice to delete $TrkC^+$ neurons. In those mice, a floxed-STOP diphtheria toxin receptor (DTR) is knocked into the advillin locus, and thus, $TrkC^{CreERT2}$-mediated recombination will result in expression of DTR solely in adult sensory ganglia. Unexpectedly, we observed 100% lethality in those mice within 48 h after injection of diphtheria toxin (DTX) (Figure 3A). To assess the extent of ablation, in particular its specificity to sensory neurons, we generated triple-transgenic $TrkC^{CreERT2}$::$Avil^{iDTR}Rosa26^{ChR2\text{-}YFP}$ to visualize the loss of $TrkC^+$ cells. After the DTX injection, we detected a complete absence of $TrkC^+$ neurons in the DRGs (Figure 3B) and innervating blood vessels (Figure 3C). Importantly, however, Th^+ fibers were still evident around vessels (red signal; Figure 3C), likely representing sympathetic neurons, as were $TrkC^+$ vSMC (yellow signal; Figure 3C).

We next investigated the effect of $TrkC^+$ neuron loss on local blood flow using laser speckle contrast imaging (LSCI) in anesthetized mice; 16 h after DTX injection, there was a significant reduction in peripheral blood flow in the skin of mice (Figures 3D and 3E), to the extent that smaller arteries were no longer detectable (reduction in vascularized area; Figure 3F), and relative perfusion in larger vessels was also reduced. During the next 16 h, this then rebounded, such that, shortly before death, the mice displayed substantially higher blood flow (Figures 3D–3F).

To investigate factors that may be contributing to lethality upon ablation of $TrkC^+$ neurons, we monitored systolic blood pressure and heart rate after injection of DTX. At 16 h after DTX injection, we observed a large decrease in blood pressure (107 ± 6 mm Hg compared with 133 ± 4 mm Hg before injection), which decreased further at the 24-h and 32-h time points (24 h: 100 ± 7 mm Hg, 32 h: 96 ± 6 mm Hg) (Figure 4A). Heart rate measurements showed a complex progression during the 48 h. Average heart rate was not different between treated mice and controls at any time point (Figure 4B). However, increases in heart rate variability (HRV) were clearly apparent at 24 (Figure 4C) and 32 h after DTX injection (Figure 4D). This was evidenced by a

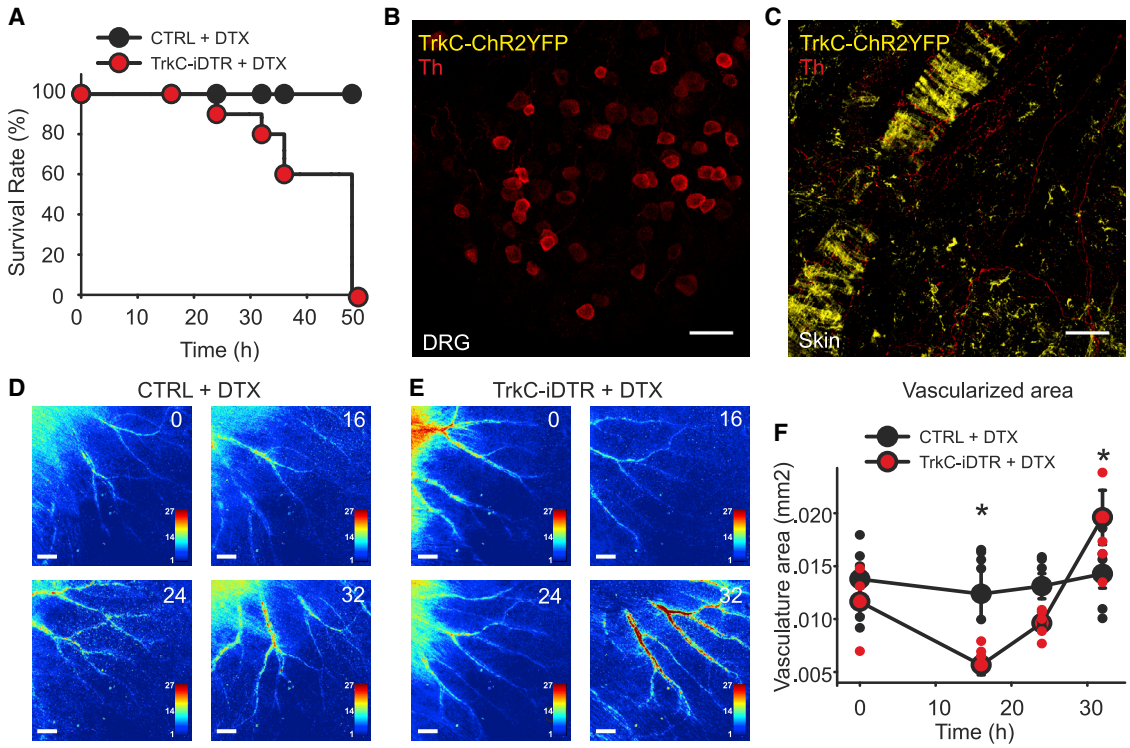

Figure 3. Loss of function in TrkC$^+$ neurons

(A) Survival rate of TrkC^{CreERT2}Avil^{iDTR} (red symbols, n = 10) and control mice (black symbols, n = 10) upon intraperitoneal administration of DTX.

(B and C) Ablation leads to a complete absence of TrkC$^+$ neurons in DRG and of TrkC$^+$/Th$^+$ fibers innervating blood vessels. Immunofluorescence with Th antibodies on DRG sections (B) and whole-mount skin (C) from TrkC^{CreERT2}::Avil^{iDTR}::Rosa26$^{ChR2\text{-}YFP}$ mice after DTX injection. Scale bars, 50 μm.

(D and E) Representative LSCI images of the ear of a control (D) and a TrkC^{CreERT2}::Avil^{iDTR} mouse (E) before DTX injection (0) and at 16, 24, and 32 h after treatment. Scale bars, 1 mm.

(F) Measurements of the vascularized area showed blood flow alteration upon ablation of TrkC$^+$ neurons. *p < 0.05.

significant increase in long-term variability over 30 min (Figures 4E, S4A, and S4B) but not in beat-to-beat, short-term variations in the signal (Figure 4F), suggesting autonomic dysregulation (Task Force of the European Society of Cardiology and the North American Society of Pacing and Electrophysiology, 1996). We also investigated the possibility that, as well as providing neuronal regulation of cardiovascular output, TrkC$^+$ neurons might supply trophic support to vSMC. Upon ablation, however, we observed no change in blood vessel integrity compared with that of controls as assessed by α-SMA immunohistochemistry (Figures S4C and S4D).

To investigate the mechanism by which TrkC$^+$ sensory neurons regulate the cardiovascular system, we took a gain-of-function approach to activate TrkC$^+$ neurons and monitored blood flow, vessel diameter, blood pressure, and heart rate upon stimulation. We used an Avil^{hM3Dq} mouse line that allows for Cre-dependent expression of the excitatory Gq-coupled designer receptor exclusively activated by designer drugs (DREADD) (Dhandapani et al., 2018). Similar to the approach taken with DTR, in these mice, a floxed-STOP hM3Dq receptor is knocked into the advillin locus, and thus, the TrkC^{CreERT2}-mediated recombination will result in expression of hM3Dq solely in adult sensory ganglia.

To monitor blood flow at the macroscopic tissue level, we injected clozapine *N*-oxide (CNO) into the paw of anesthetized TrkC^{CreERT2}::Avil^{hM3Dq} mice and imaged the vasculature for 30 min using LSCI (Figure 5A). At 10 min post-injection, a significant reduction in vascularized area and perfusion rate was evident, which progressively decreased such that after 20 min, the vasculature became essentially undetectable (Figures 5B and 5C). To examine that further at the microscopic, single-vessel level, we performed *in vivo* three-photon (3P) microscopy in conjunction with optogenetic activation of TrkC$^+$ neurons in anesthetized TrkC^{CreERT2}::Rosa26$^{ChR2\text{-}YFP}$ mice injected intrathecally with 45 ng 4-hydroxytamoxifen. We selected the ear of mice for these experiments because we were unable to detect TrkC$^+$ proprioceptors and Aβ field mechanoreceptors in that area, whereas TrkC$^+$/TH$^+$ perivascular neurons were evident (Figure S5), thus, allowing for selective activation of TrkC$^+$ vasculature afferents. Intriguingly, upon optical stimulation, we observed a significant decrease in vessel cross-sectional area in TrkC^{CreERT2}::Rosa26$^{ChR2\text{-}YFP}$ mice, which was not apparent in control animals (Figures 5D and 5E; Video S1). To confirm that this was associated with a reduction in blood flow, as seen in LCSI experiments, red blood cell velocity was calculated from spatially windowed 3P line-scan data. As shown in Figures

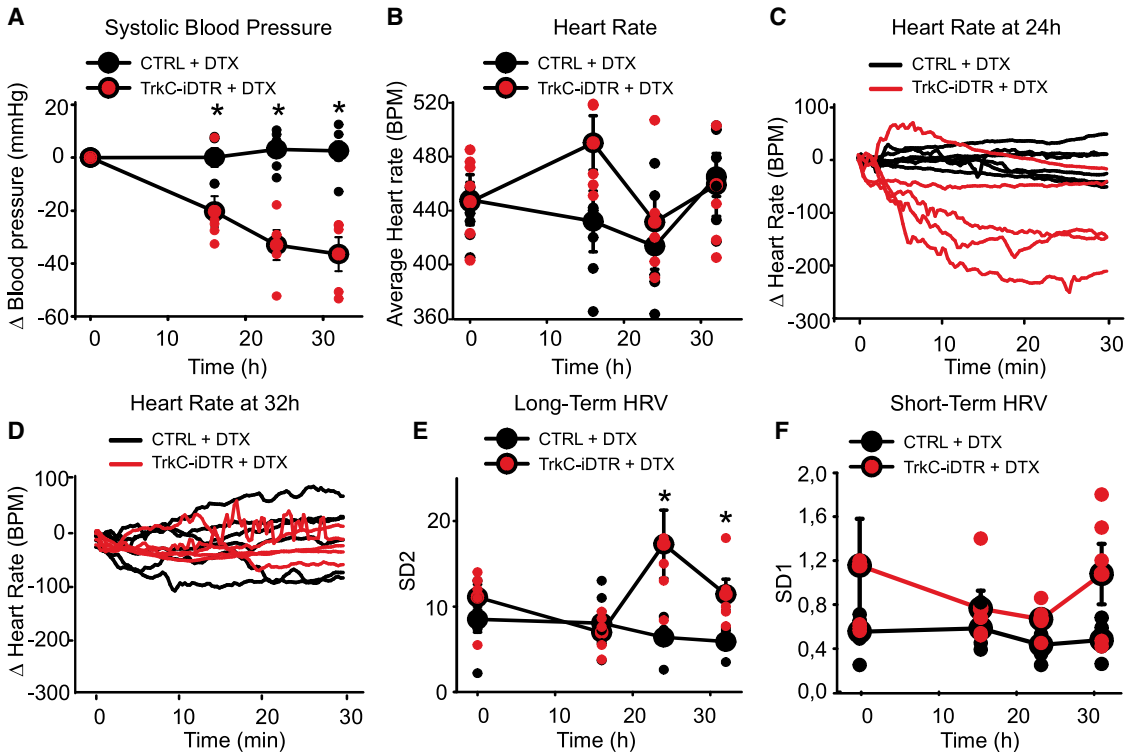

Figure 4. Ablation of TrkC$^+$ neurons leads to blood pressure and heart rate alterations

(A) Upon systemic injection of DTX, TrkC^{CreERT2}::Avil^{iDTR} mice display a decrease in blood pressure (red symbols, n = 5), whereas control mice (black symbols, n = 6) are not affected. *p < 0.001.

(B) Average heart rate in TrkC^{CreERT2}::Avil^{iDTR} mice (red symbols, n = 5) after DTX injections at different time points over 30 min compared with control mice (black symbols, n = 6).

(C and D) Fluctuations in heart rate for individual mice over 30 min at 24 (C) and 32 (D) h after DTX injection.

(E) Long-term heart rate variability derived from the length of the major (SD2) axis of Poincaré plots at different time points after injection of DTX. Significant differences in variability are evident in TrkC^{CreERT2}::Avil^{iDTR} mice compared with controls at 24 and 32 h after injection. *p < 0.05.

(F) Short-term variability derived from the length of the minor (SD1) axis of the Poincaré plots at different time points after injection of DTX in TrkC^{CreERT2}::Avil^{iDTR} and control mice.

5F and 5G and Videos S2 and S3, optical stimulation provoked a dramatic and persistent decrease in blood flow, such that individual red blood cells became clearly visible at the imaging frame rate.

To investigate whether TrkC$^+$ neurons exert their effects on blood vessels locally, we next performed confocal live imaging in an isolated *ex vivo* preparation of the hind limb skin in which spinal reflex arcs were disrupted (Figure 5H). We never detected changes in vessel size upon activation of TrkC$^+$ neurons using either chemogenetic or optogenetic stimulation (Figures 5I and 5J; Videos S4 and S5). However, direct activation of TrkC$^+$ vSMC expressing ChR2 using optogenetics or via application of norepinephrine provoked robust constriction of vessels, suggesting that the preparation was viable, even in the absence of blood flow (Figures 5K and 5L; Videos S6 and S7). Thus, TrkC$^+$ neurons are unlikely to exert an efferent function via axon reflex, and they do not appear to act through local connections with sympathetic neurons.

We further assessed the influence of TrkC$^+$ neuronal activation on systolic blood pressure and heart rate (Figure 6A). We used the DREADD agonist 21 (C21) (Chen et al., 2015) to avoid off-target systemic effects associated with metabolism of CNO to clozapine (Gomez et al., 2017). C21 was injected intraperitoneally into TrkC^{CreERT2}::Avil^{hM3Dq} mice, and within 10 min, we observed a substantial increase in blood pressure from 117 ± 3 mm Hg to 154 ± 2 mm Hg, which persisted for 30 min (Figure 6B). Average heart rate also increased significantly over the same time course (Figure 6C), and heart rate variability became evident (Figure 6D). This was accompanied by an increase in long- but not short-term measures of HRV (Figures 6E, 6F, and S6). We next treated mice with the β-adrenergic receptor-blocker propranolol to inhibit sympathetic input (Figure 6A). In the presence of propranolol, C21 did not provoke any changes in blood pressure (Figure 6B), heart rate (Figures 6C and 6D), or variability (Figures 6E, 6F, and S6), indicating that TrkC$^+$ neurons signal via the sympathetic nervous system to regulate cardiovascular output.

Finally, we investigated the consequences of local activation of TrkC$^+$ neurons and subsequent reductions of peripheral blood flow, on sensory behavior. CNO was injected subcutaneously in the paw and responses to mechanical and thermal stimulation of the skin were monitored (Figure 7A). We observed a striking reduction in mechanical thresholds after CNO injection

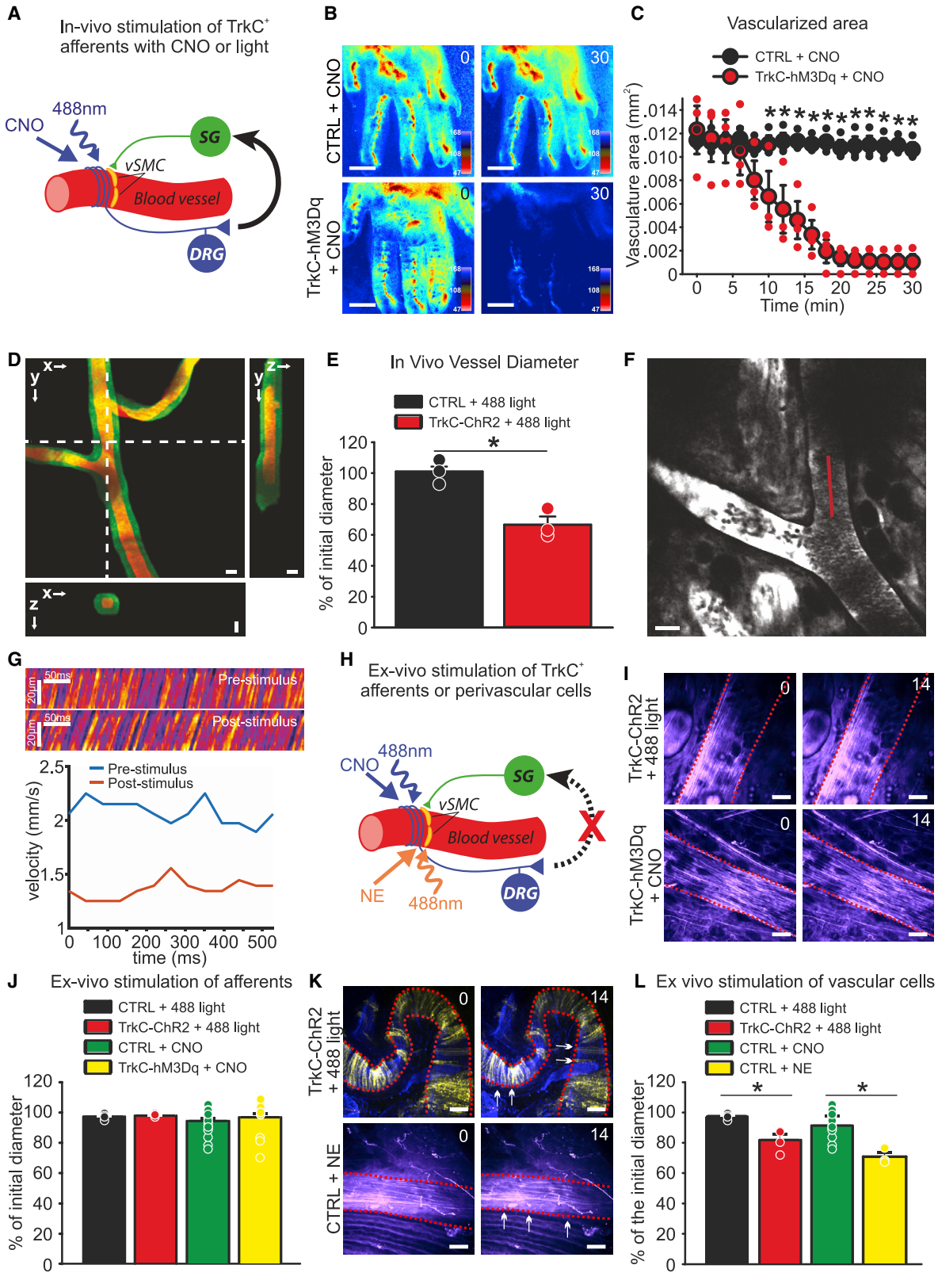

(legend on next page)

(Figure 7B), such that 10 min after injection, mice became hypersensitive to the lightest of punctate stimuli (Figure 7C). Responses to dynamic brushing stimuli and thermal stimuli were not altered by CNO (Figures 7D–7F).

DISCUSSION

Here, we describe a population of peripheral neurons marked by TrkC and Th that have cell bodies in the spinal ganglia and project to distal blood vessels. We demonstrate that ablation of TrkC$^+$ neurons leads to rapid reductions in blood flow to the skin and that, over the course of 48 h, this effect is accompanied by a catastrophic drop in blood pressure and increased heart rate lability, which may underlie the death of mice. Moreover, we show that activation of those neurons provokes vasoconstriction and increased blood pressure and heart rate variability, which is dependent upon β-adrenergic signaling, implicating a role for the sympathetic nervous system. Intriguingly, activation of the neurons also provokes a profound and rapid hypersensitivity to punctate mechanical stimulation of the skin.

Our data indicate that there is a discrete population of TrkC$^+$ DRG neurons that innervate the vasculature, which are molecularly, anatomically, and functionally distinct from previously described perivascular sensory neurons. In contrast to peptidergic neurons, TrkC$^+$ neurons do not express CGRP, are not activated by capsaicin, and have no apparent efferent function through axon reflexes (Bayliss, 1901; Bruce, 1913; Gibbins et al., 1985; Vass et al., 2004). Upon stimulation, they also provoke vasoconstriction rather than vasodilation (Burnstock, 2007; Kawasaki et al., 1988). Thus, functionally, they more closely resemble baroreceptors, and indeed, they appear to contribute to a baroreceptor-reflex-like arc to control arterial pressure. However, baroreceptors have their cell bodies in the cervical ganglia and project to the aortic arch and carotid artery (Kirchheim, 1976), whereas TrkC$^+$ neurons are located in the spinal ganglia and project to the distal arteries. Moreover, baroreceptor stimulation provides negative feedback to the cardiovascular output (Coleridge and Coleridge, 1980), whereas activation of TrkC$^+$ neurons has opposing effects and raises the blood pressure and heart rate. Ablation studies also reveal differences between TrkC$^+$ neurons and other populations of perivascular afferents. Thus, depletion of the peptidergic vascular afferent nerves with capsaicin does not disrupt baroreceptor reflexes (Furness et al., 1982), whereas surgical denervation of baroreceptors results in blood pressure variability, often accompanied by an increase in arterial blood pressure (Heusser et al., 2005; Ito and Scher, 1981; Robertson et al., 1993; Rodrigues et al., 2011; Stocker et al., 2019; Sved et al., 1997). In contrast, our data show that ablation of TrkC$^+$ neurons leads to a significant decrease in systolic blood pressure, followed by death of mice within 48 h. We, thus, speculate that TrkC$^+$ vascular innervation is essential for integrating information on perfusion status from distal tissues and providing positive feedback to the cardiovascular system. Investigating how these neurons signal and respond under different physiological conditions and determining whether they exist in other species beyond mice are important questions for future studies.

A limitation of our genetic manipulation experiments is that we target all TrkC$^+$ sensory neurons when using the TrkC^{CreERT2} driver and not just TrkC$^+$/Th$^+$ afferents. TrkC also marks Aβ field mechanoreceptors in the skin and proprioceptors in the muscle and tendons, and indeed, only around a third of all TrkC$^+$ sensory neurons are positive for Th. Presumably, however, manipulation of cutaneous mechanoreceptors or proprioceptors would be unlikely to provoke robust effects on vascular parameters or ultimately lead to lethality upon ablation. In early experiments, we attempted to genetically isolate the TrkC$^+$/Th$^+$ population using intersectional approaches but were unsuccessful because of a lack of efficiency and specificity of the available Th drivers (see method details). To address that issue, we, therefore, performed optogenetic experiments in the ears of mice, selecting a region

Figure 5. Activation of TrkC$^+$ neurons

(A) Schematic showing *in vivo* circuit activated by CNO in TrkC^{CreERT2}::Avil^{hM3Dq} mice, or 488 nm of light in TrkC^{CreERT2}::Rosa26$^{ChR2\text{-}YFP}$ mice injected intrathecally with 45 ng of 4-hydroxytamoxifen.

(B) Representative LSCI images showing blood vessels in the hind paw of control mice (top panels) or TrkC^{CreERT2}::Avil^{hM3Dq} mice (bottom panels) treated locally with CNO imaged before and 30 min after the treatment. Scale bars, 1 mm.

(C) Measurements of the vascularized area of LSCI images showing blood flow reduction upon local activation of TrkC$^+$ neurons with CNO (red symbols, *$p < 0.001$, $n = 3$).

(D) Three-photon volumetric image of blood vessels in TrkC^{CreERT2}::Rosa26$^{ChR2\text{-}YFP}$ mouse ear labeled with dextran-fluorescein. Maximum-intensity projection along the lateral imaging plane (x/y) and orthogonal projection of three-dimensional (3D) volume along lines indicated in the (x/y) image by the white, dotted line. Image of green-labeled artery was acquired before the optogenetic stimulus, and red was after the stimulus. Scale bar, 25 μm.

(E) Quantification of blood vessel diameter after optical stimulation. *$p < 0.005$.

(F) Three-photon image of blood vessels in the mouse ear labeled with dextran-fluorescein. Red line indicates the laser scan path used to measure and calculate red blood cell velocity. Line-scans were acquired at 666 Hz.

(G) Top, line scans generated from the path indicated by the red line in (F) can be stacked as a space-time (x/t) plot, in which the apparent angle is proportional to flow velocity. The images show ~500 ms of data collection before and after optogenetic stimulation, respectively. Bottom, red blood cell velocity before and after stimulation. Velocity was calculated based on radon analysis of spatially windowed space-time plot data (window size, 50 ms).

(H) Schematic showing *ex vivo* stimulation of TrkC$^+$ afferents (blue) by CNO in TrkC^{CreERT2}::Avil^{hM3Dq} mice or 488 nm of illumination in TrkC^{CreERT2}::Rosa26$^{ChR2\text{-}YFP}$ mice injected intrathecally or *ex vivo* stimulation of vSMC (orange) by norepinephrine (NE) or 488 nm light in TrkC^{CreERT2}::Rosa26$^{ChR2\text{-}YFP}$ mice injected systemically.

(I) Representative images of blood vessels from an *ex vivo* skin-nerve preparation before and 14 min after optogenetic activation of TrkC$^+$ neurons (top panels) or application of CNO (bottom panels). Scale bars, 25 μm.

(J) Quantification of blood vessel diameter after *ex vivo* stimulation of TrkC$^+$ afferents with 488 nm of light or CNO application.

(K) Representative images of blood vessels before and 14 min after optogenetic activation of vSMC (top panels) or application of norepinephrine (bottom panels). Dotted lines indicate blood vessel perimeter; arrows indicate shrinkage. Scale bars, 25 μm.

(L) Quantification of blood vessel diameter after *ex vivo* stimulation of TrkC$^+$ vSMC with 488 nm or light or norepinephrine application. *$p < 0.01$.

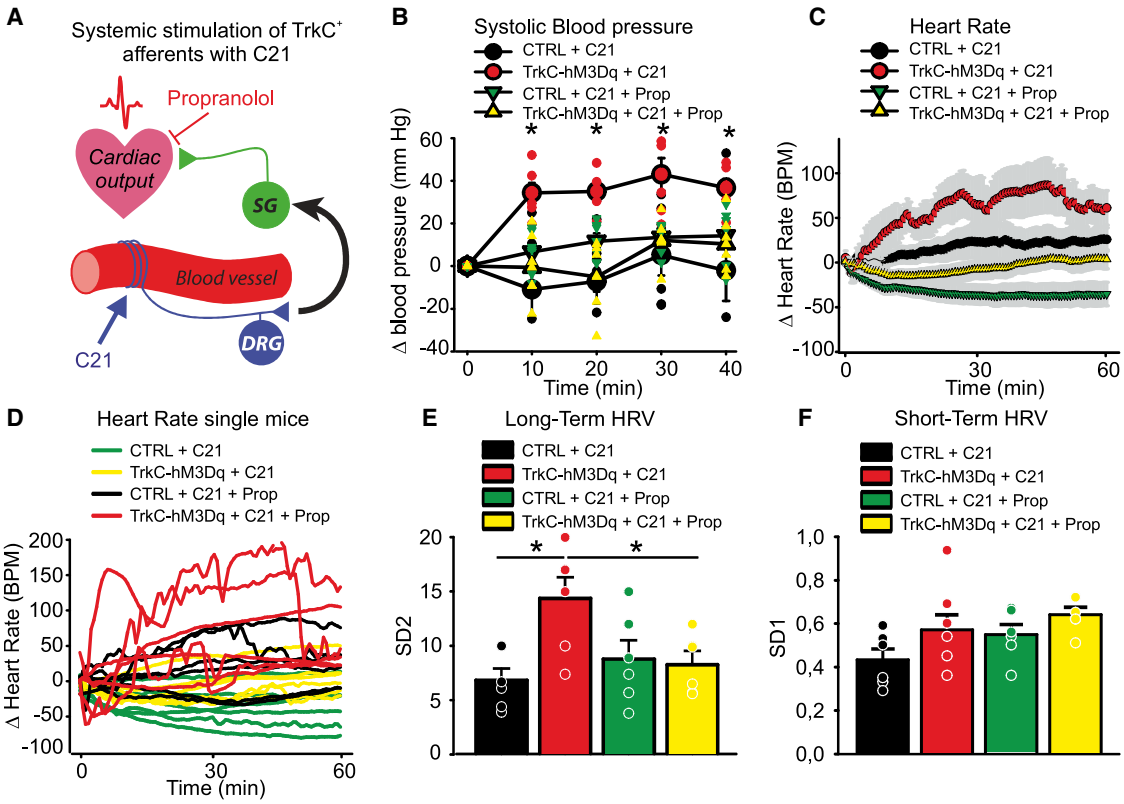

Figure 6. Systemic chemogenetic activation of TrkC$^+$ neurons leads to blood pressure and heart rate alterations

(A) Schematic showing circuit activated by C21 *in vivo*.

(B) Systemic injection of C21 in TrkC^{CreERT2}::Avil^{hM3Dq} mice leads to elevated blood pressure (red symbols, n = 6) compared with control mice (black symbols, n = 6). *p < 0.01. This is reverted by co-administration of propranolol (yellow symbols, n = 6).

(C) TrkC^{CreERT2}::Avil^{hM3Dq} mice (red symbols, n = 6) treated systemically with C21 display increased average heart rate compared with mice co-treated with propranolol (yellow symbols, n = 6) or control mice (black and green symbols).

(D) Fluctuations in heart rate in individual mice are apparent in TrkC^{CreERT2}::Avil^{hM3Dq} mice treated with C21 (red lines) but not in mice co-treated with propranolol (yellow lines) or control animals (black and green lines).

(E) Long-term heart rate variability derived from the length of the major (SD2) axis of Poincaré plots in TrkC^{CreERT2}::Avil^{hM3Dq} mice treated with C21, C21 plus propranolol, or in control mice. *p < 0.05.

(F) Short-term heart rate variability derived from the length of the minor (SD1) axis of Poincaré plots in TrkC^{CreERT2}::Avil^{hM3Dq} mice treated with C21, C21 plus propranolol, or in control mice.

of tissue that we observed was devoid of TrkC$^+$ proprioceptors and Aβ field receptors but that did contain TrkC$^+$/Th$^+$ perivascular neurons. Imaging directly from the vasculature, we found that optical stimulation of TrkC$^+$ afferents provoked robust effects on local vessel diameter and blood flow. In future work, it will be interesting to examine whether local stimulation is also able to evoke changes in blood flow in other areas (for example, in the contralateral ear) or, indeed, produce systemic changes in heart rate and blood pressure.

In addition to its expression in a subpopulation of TrkC$^+$ neurons, Th is also a marker of sympathetic neurons, where it functions as the enzyme that catalyzes the biosynthesis of catecholamines, such as norepinephrine. This may explain why these neurons have not been described previously, because it would be impossible to distinguish them from perivascular sympathetic neurons based upon their expression of Th. Importantly, we find no evidence for TrkC^{CreERT2}-mediated recombination in sympathetic ganglia, whereas it is coexpressed with Th in DRGs. This implies that TrkC$^+$/Th$^+$ nerves are indeed of sensory origin with their cell bodies in the spinal ganglia. This raises an important question as to whether Th has an enzymatic role in sensory neurons and whether it can synthesize and release norepinephrine for a direct action on blood vessels. Our *in vitro* imaging data suggest that this is not the case because both optogenetic and chemogenetic activation of the neurons did not elicit a change in blood vessel diameter in isolated tissues (although an important caveat here is that blood flow may be required to trigger a response). Similarly, analysis of RNA-seq data reveals that the other enzymes required for catecholamine synthesis are not detected in TrkC$^+$/Th$^+$ neurons (Figure S1N; Zeisel et al., 2018) consistent with previous reports (Brumovsky et al., 2006; Kummer et al., 1990; Price, 1985; Vega et al., 1991). Future studies, that use conditional knockout of Th in TrkC neurons, for example, will determine what, if any, the functional role of Th is in these neurons.

Our *in vivo* live imaging data revealed robust effects of TrkC$^+$ neuronal stimulation on blood flow and vessel diameter. Using

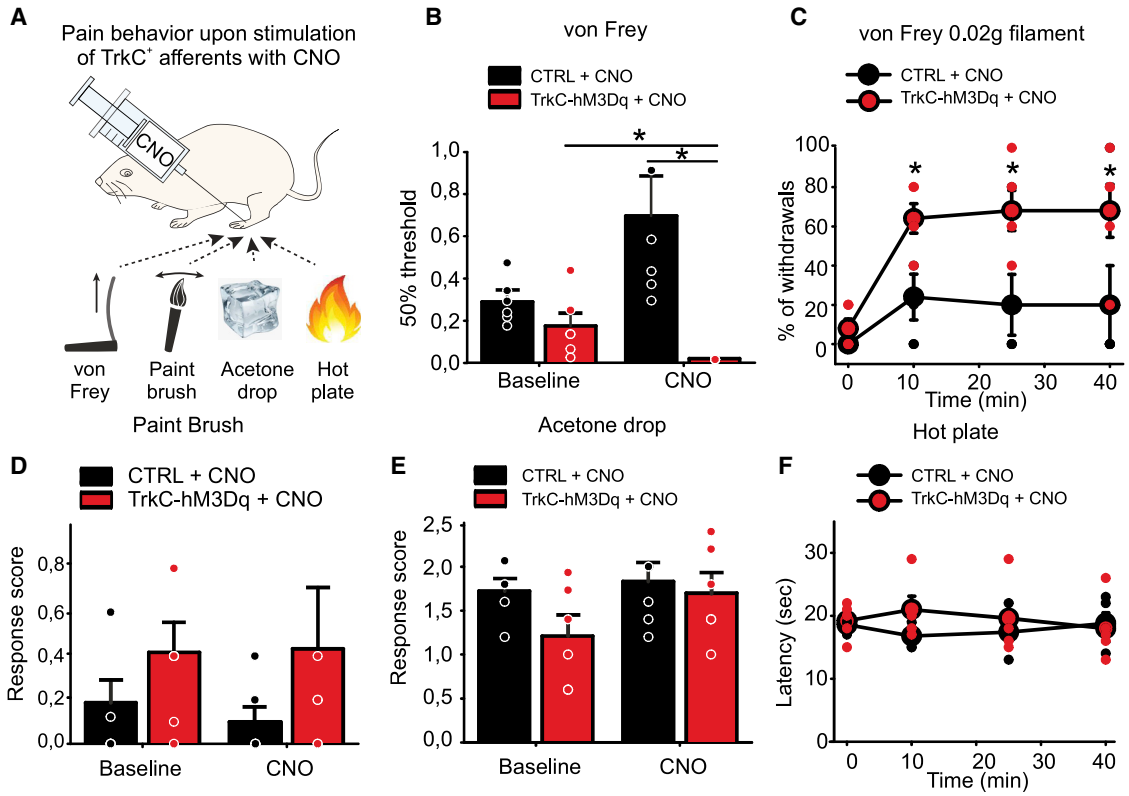

Figure 7. Behavioral responses to mechanical and thermal stimulation upon chemogenetic activation of TrkC$^+$ sensory neurons

(A) Schematic of behavioral tests performed after local injection of CNO.

(B and C) TrkC^{CreERT2}::Avil^{hM3Dq} developed hypersensitivity to punctate mechanical stimuli (n = 6) *p < 0.05 (B), which started 10 min after CNO local treatment and persisted for more than 40 min (C) (0.02 g filament, n = 5). *p < 0.05.

(D) Local intraplantar injection of CNO in TrkC^{CreERT2}::Avil^{hM3Dq} mice does not provoke mechanical hypersensitivity to dynamic mechanical stimuli (paintbrush, n = 6).

(E and F) Thermal sensitivity as assayed by the acetone drop test (n = 6) (E) and hot-plate test (n = 5) (F) was not different between TrkC^{CreERT2}::Avil^{hM3Dq} (red symbols) and control mice (black symbols) treated with CNO.

LCSI and 3P imaging across spatial scales, we observed a substantial decrease in blood flow to the skin and a reduction in vessel cross-sectional area. This indicates that vasoconstriction provoked by activation of TrkC$^+$ neurons may divert regional blood flow away from peripheral tissues. Accordingly, in LCSI experiments, we observed an almost complete loss of the detectable vasculature upon local stimulation, which commenced in the distal toes and proceeded proximally over time. Intriguingly, DTX-mediated ablation also led to an initial decrease in blood flow, albeit with a prolonged time course compared with that of the stimulation experiments. This could reflect complex effects on blood perfusion because the ablation is occurring ubiquitously and slowly over the course of 2 days. Thus, an initial drop may be due to compensation for reduced blood pressure. As further TrkC$^+$ neurons are lost, that compensation may not be maintained, hence, the increase in perfusion before death of the animals.

One consequence of reduced peripheral perfusion would be tissue hypoxia and acidosis leading to ischemic pain (Anitescu, 2018). Accordingly, we observed a profound mechanical hypersensitivity upon local stimulation of TrkC$^+$ neurons, which paralleled the reduction in vascularized area. Of note, alterations in neuronal control of vasculature have been associated with a number of painful conditions, including diabetic neuropathy, migraine, Raynaud's disease, and fibromyalgia (Albrecht et al., 2013; Burnstock, 2008; Cooke and Marshall, 2005; Edvinsson et al., 2019; Jacobs and Dussor, 2016; Pietrobon and Moskowitz, 2013; Queme et al., 2017; Schmidt, 2014). To date, most studies have considered only the contribution of autonomic and peptidergic sensory neurons to those conditions. However, the identification of a class of non-peptidergic perivascular sensory neurons now opens up the possibility that they may also have a role in vascular-associated pain. Identification of TrkC as a marker of those neurons will now enable further studies to trace their anatomical connections with the sympathetic nervous system and help to elucidate their role in regulating peripheral blood flow under basal conditions and in disease.

STAR★METHODS

Detailed methods are provided in the online version of this paper and include the following:

- KEY RESOURCES TABLE
- RESOURSE AVAILABILITY

SUPPLEMENTAL INFORMATION

Supplemental information can be found online at https://doi.org/10.1016/j.celrep.2021.109191.

ACKNOWLEDGMENTS

We thank Philip Hublitz of EMBL Gene Expression Services, Pedro Moreira of EMBL Transgenic Services, and Violetta Paribeni for technical support of our work.

AUTHOR CONTRIBUTIONS

C.M., L.C., S.J.B., L.L.S., A.W., F.J.T., B.C., A.B., J.S., T.F., L.K.S., B.D., and J.S. acquired data and performed analysis; K.M.B. developed the computational analysis methods for LSCI; R.P., S.G.L., and P.A.H. gave feedback on experimental aspects, supervised experimental approaches, and implemented the data interpretation; L.C. prepared the figures; and P.A.H. designed the study with help from C.M. and L.C. and wrote the manuscript.

DECLARATION OF INTERESTS

The authors declare no competing interests.

Received: January 17, 2020
Revised: April 14, 2020
Accepted: May 9, 2021
Published: June 1, 2021

REFERENCES

Abrahamsen, B., Zhao, J., Asante, C.O., Cendan, C.M., Marsh, S., Martinez-Barbera, J.P., Nassar, M.A., Dickenson, A.H., and Wood, J.N. (2008). The cell and molecular basis of mechanical, cold, and inflammatory pain. Science *321*, 702–705.

Adelson, D.W., Wei, J.Y., and Kruger, L. (1997). Warm-sensitive afferent splanchnic C-fiber units in vitro. J. Neurophysiol. *77*, 2989–3002.

Albrecht, P.J., Hou, Q., Argoff, C.E., Storey, J.R., Wymer, J.P., and Rice, F.L. (2013). Excessive peptidergic sensory innervation of cutaneous arteriole-venule shunts (AVS) in the palmar glabrous skin of fibromyalgia patients: implications for widespread deep tissue pain and fatigue. Pain Med. *14*, 895–915.

Anitescu, M. (2018). Ischemic pain. In Fundamentals of Pain Medicine, J. Cheng and R.W. Rosenquist, eds. (Springer International Publishing), pp. 141–151.

Arcourt, A., Gorham, L., Dhandapani, R., Prato, V., Taberner, F.J., Wende, H., Gangadharan, V., Birchmeier, C., Heppenstall, P.A., and Lechner, S.G. (2017). Touch receptor-derived sensory information alleviates acute pain signaling and fine-tunes nociceptive reflex coordination. Neuron *93*, 179–193.

Bai, L., Lehnert, B.P., Liu, J., Neubarth, N.L., Dickendesher, T.L., Nwe, P.H., Cassidy, C., Woodbury, C.J., and Ginty, D.D. (2015). Genetic identification of an expansive mechanoreceptor sensitive to skin stroking. Cell *163*, 1783–1795.

Bayliss, W.M. (1901). On the origin from the spinal cord of the vaso-dilator fibres of the hind-limb, and on the nature of these fibres. J. Physiol. *26*, 173–209.

Bessou, P., and Perl, E.R. (1966). Amovement receptor of the small intestine. J. Physiol. *182*, 404–426.

Breitman, M.L., Clapoff, S., Rossant, J., Tsui, L.C., Glode, L.M., Maxwell, I.H., and Bernstein, A. (1987). Genetic ablation: targeted expression of a toxin gene causes microphthalmia in transgenic mice. Science *238*, 1563–1565.

Bruce, A.N. (1913). Vaso-dilator axon-reflexes. Q. J. Exp. Physiol. *6*, 339–354.

Brumovsky, P., Villar, M.J., and Hökfelt, T. (2006). Tyrosine hydroxylase is expressed in a subpopulation of small dorsal root ganglion neurons in the adult mouse. Exp. Neurol. *200*, 153–165.

Buch, T., Heppner, F.L., Tertilt, C., Heinen, T.J., Kremer, M., Wunderlich, F.T., Jung, S., and Waisman, A. (2005). A Cre-inducible diphtheria toxin receptor mediates cell lineage ablation after toxin administration. Nat. Methods *2*, 419–426.

Burnstock, G. (2007). Physiology and pathophysiology of purinergic neurotransmission. Physiol. Rev. *87*, 659–797.

Burnstock, G. (2008). Dual control of vascular tone and remodelling by ATP released from nerves and endothelial cells. Pharmacol. Rep. *60*, 12–20.

Burnstock, G., and Ralevic, V. (1994). New insights into the local regulation of blood flow by perivascular nerves and endothelium. Br. J. Plast. Surg. *47*, 527–543.

Cavanaugh, D.J., Lee, H., Lo, L., Shields, S.D., Zylka, M.J., Basbaum, A.I., and Anderson, D.J. (2009). Distinct subsets of unmyelinated primary sensory fibers mediate behavioral responses to noxious thermal and mechanical stimuli. Proc. Natl. Acad. Sci. USA *106*, 9075–9080.

Chaplan, S.R., Bach, F.W., Pogrel, J.W., Chung, J.M., and Yaksh, T.L. (1994). Quantitative assessment of tactile allodynia in the rat paw. J. Neurosci. Methods *53*, 55–63.

Chen, X., Choo, H., Huang, X.P., Yang, X., Stone, O., Roth, B.L., and Jin, J. (2015). The first structure-activity relationship studies for designer receptors exclusively activated by designer drugs. ACS Chem. Neurosci. *6*, 476–484.

Coleridge, H.M., and Coleridge, J.C. (1980). Cardiovascular afferents involved in regulation of peripheral vessels. Annu. Rev. Physiol. *42*, 413–427.

Cooke, J.P., and Marshall, J.M. (2005). Mechanisms of Raynaud's disease. Vasc. Med. *10*, 293–307.

Copray, J.C., Mantingh-Otter, I.J., and Brouwer, N. (1994). Expression of calcium-binding proteins in the neurotrophin-3-dependent subpopulation of rat embryonic dorsal root ganglion cells in culture. Brain Res. Dev. Brain Res. *81*, 57–65.

Delfini, M.C., Mantilleri, A., Gaillard, S., Hao, J., Reynders, A., Malapert, P., Alonso, S., François, A., Barrere, C., Seal, R., et al. (2013). TAFA4, a

chemokine-like protein, modulates injury-induced mechanical and chemical pain hypersensitivity in mice. Cell Rep. *5*, 378–388.

Dhandapani, R., Arokiaraj, C.M., Taberner, F.J., Pacifico, P., Raja, S., Nocchi, L., Portulano, C., Franciosa, F., Maffei, M., Hussain, A.F., et al. (2018). Control of mechanical pain hypersensitivity in mice through ligand-targeted photoablation of TrkB-positive sensory neurons. Nat. Commun. *9*, 1640.

Duan, B., Cheng, L., Bourane, S., Britz, O., Padilla, C., Garcia-Campmany, L., Krashes, M., Knowlton, W., Velasquez, T., Ren, X., et al. (2014). Identification of spinal circuits transmitting and gating mechanical pain. Cell *159*, 1417–1432.

Edvinsson, L., Haanes, K.A., and Warfvinge, K. (2019). Does inflammation have a role in migraine? Nat. Rev. Neurol. *15*, 483–490.

Furness, J.B., Elliott, J.M., Murphy, R., Costa, M., and Chalmers, J.P. (1982). Baroreceptor reflexes in conscious guinea-pigs are unaffected by depletion of cardiovascular substance P nerves. Neurosci. Lett. *32*, 285–290.

Gibbins, I.L., Furness, J.B., Costa, M., MacIntyre, I., Hillyard, C.J., and Girgis, S. (1985). Co-localization of calcitonin gene-related peptide-like immunoreactivity with substance P in cutaneous, vascular and visceral sensory neurons of guinea pigs. Neurosci. Lett. *57*, 125–130.

Gnyawali, S.C., Blum, K., Pal, D., Ghatak, S., Khanna, S., Roy, S., and Sen, C.K. (2017). Retooling laser speckle contrast analysis algorithm to enhance non-invasive high resolution laser speckle functional imaging of cutaneous microcirculation. Sci. Rep. *7*, 41048.

Gomez, J.L., Bonaventura, J., Lesniak, W., Mathews, W.B., Sysa-Shah, P., Rodriguez, L.A., Ellis, R.J., Richie, C.T., Harvey, B.K., Dannals, R.F., et al. (2017). Chemogenetics revealed: DREADD occupancy and activation via converted clozapine. Science *357*, 503–507.

Gompf, H.S., Budygin, E.A., Fuller, P.M., and Bass, C.E. (2015). Targeted genetic manipulations of neuronal subtypes using promoter-specific combinatorial AAVs in wild-type animals. Front. Behav. Neurosci. *9*, 152.

Haupt, P., Jänig, W., and Kohler, W. (1983). Response pattern of visceral afferent fibres, supplying the colon, upon chemical and mechanical stimuli. Pflugers Arch. *398*, 41–47.

Heusser, K., Tank, J., Luft, F.C., and Jordan, J. (2005). Baroreflex failure. Hypertension *45*, 834–839.

Ito, C.S., and Scher, A.M. (1981). Hypertension following arterial baroreceptor denervation in the unanesthetized dog. Circ. Res. *48*, 576–591.

Jacobs, B., and Dussor, G. (2016). Neurovascular contributions to migraine: moving beyond vasodilation. Neuroscience *338*, 130–144.

Kawasaki, H., Takasaki, K., Saito, A., and Goto, K. (1988). Calcitonin gene-related peptide acts as a novel vasodilator neurotransmitter in mesenteric resistance vessels of the rat. Nature *335*, 164–167.

Kirchheim, H.R. (1976). Systemic arterial baroreceptor reflexes. Physiol. Rev. *56*, 100–177.

Kong, L., and Cui, M. (2013). A high throughput (>90%), large compensation range, single-prism femtosecond pulse compressor. arXiv, 1306:5011v1.

Kummer, W., Gibbins, I.L., Stefan, P., and Kapoor, V. (1990). Catecholamines and catecholamine-synthesizing enzymes in guinea-pig sensory ganglia. Cell Tissue Res. *261*, 595–606.

Lembeck, F., and Holzer, P. (1979). Substance P as neurogenic mediator of antidromic vasodilation and neurogenic plasma extravasation. Naunyn Schmiedebergs Arch. Pharmacol. *310*, 175–183.

Li, L., Rutlin, M., Abraira, V.E., Cassidy, C., Kus, L., Gong, S., Jankowski, M.P., Luo, W., Heintz, N., Koerber, H.R., et al. (2011). The functional organization of cutaneous low-threshold mechanosensory neurons. Cell *147*, 1615–1627.

Liu, J., Merlie, J.P., Todd, R.D., and O'Malley, K.L. (1997). Identification of cell type-specific promoter elements associated with the rat tyrosine hydroxylase gene using transgenic founder analysis. Brain Res. Mol. Brain Res. *50*, 33–42.

Palmiter, R.D., Behringer, R.R., Quaife, C.J., Maxwell, F., Maxwell, I.H., and Brinster, R.L. (1987). Cell lineage ablation in transgenic mice by cell-specific expression of a toxin gene. Cell *50*, 435–443.

Pietrobon, D., and Moskowitz, M.A. (2013). Pathophysiology of migraine. Annu. Rev. Physiol. *75*, 365–391.

Price, J. (1985). An immunohistochemical and quantitative examination of dorsal root ganglion neuronal subpopulations. J. Neurosci. *5*, 2051–2059.

Queme, L.F., Ross, J.L., and Jankowski, M.P. (2017). Peripheral mechanisms of ischemic myalgia. Front. Cell. Neurosci. *11*, 419.

Robertson, D., Hollister, A.S., Biaggioni, I., Netterville, J.L., Mosqueda-Garcia, R., and Robertson, R.M. (1993). The diagnosis and treatment of baroreflex failure. N. Engl. J. Med. *329*, 1449–1455.

Rodrigues, F.L., de Oliveira, M., Salgado, H.C., and Fazan, R., Jr. (2011). Effect of baroreceptor denervation on the autonomic control of arterial pressure in conscious mice. Exp. Physiol. *96*, 853–862.

Rodríguez-Liñares, L., Lado, M.J., Vila, X.A., Méndez, A.J., and Cuesta, P. (2014). gHRV: Heart rate variability analysis made easy. Comput. Methods Programs Biomed. *116*, 26–38.

Schmidt, R.E. (2014). Autonomic neuropathy in experimental models of diabetes mellitus. Handb. Clin. Neurol. *126*, 579–602.

Schneider, C.A., Rasband, W.S., and Eliceiri, K.W. (2012). Nat. Methods *9*, 671–675.

Stantcheva, K.K., Iovino, L., Dhandapani, R., Martinez, C., Castaldi, L., Nocchi, L., Perlas, E., Portulano, C., Pesaresi, M., Shirlekar, K.S., et al. (2016). A subpopulation of itch-sensing neurons marked by Ret and somatostatin expression. EMBO Rep. *17*, 585–600.

Stocker, S.D., Sved, A.F., and Andresen, M.C. (2019). Missing pieces of the Piezo1/Piezo2 baroreceptor hypothesis: an autonomic perspective. J. Neurophysiol. *122*, 1207–1212.

Sved, A.F., Schreihofer, A.M., and Kost, C.K., Jr. (1997). Blood pressure regulation in baroreceptor-denervated rats. Clin. Exp. Pharmacol. Physiol. *24*, 77–82.

Task Force of the European Society of Cardiology; North American Society of Pacing and Electrophysiology (1996). Heart rate variability: standards of measurement, physiological interpretation and clinical use. Circulation *93*, 1043–1065.

Thomas, G.D. (2011). Neural control of the circulation. Adv. Physiol. Educ. *35*, 28–32.

Vass, Z., Dai, C.F., Steyger, P.S., Jancsó, G., Trune, D.R., and Nuttall, A.L. (2004). Co-localization of the vanilloid capsaicin receptor and substance P in sensory nerve fibers innervating cochlear and vertebro-basilar arteries. Neuroscience *124*, 919–927.

Vega, J.A., Amenta, F., Hernandez, L.C., and del Valle, M.E. (1991). Presence of catecholamine-related enzymes in a subpopulation of primary sensory neurons in dorsal root ganglia of the rat. Cell. Mol. Biol. *37*, 519–530.

Wehrwein, E.A., and Joyner, M.J. (2013). Regulation of blood pressure by the arterial baroreflex and autonomic nervous system. Handb. Clin. Neurol. *117*, 89–102.

Westcott, E.B., and Segal, S.S. (2013). Perivascular innervation: a multiplicity of roles in vasomotor control and myoendothelial signaling. Microcirculation *20*, 217–238.

Zeisel, A., Hochgerner, H., Lönnerberg, P., Johnsson, A., Memic, F., van der Zwan, J., Häring, M., Braun, E., Borm, L.E., La Manno, G., et al. (2018). Molecular architecture of the mouse nervous system. Cell *174*, 999–1014.e22.

Zeng, W.Z., Marshall, K.L., Min, S., Daou, I., Chapleau, M.W., Abboud, F.M., Liberles, S.D., and Patapoutian, A. (2018). PIEZOs mediate neuronal sensing of blood pressure and the baroreceptor reflex. Science *362*, 464–467.

STAR★METHODS

KEY RESOURCES TABLE

REAGENT or RESOURCE	SOURCE	IDENTIFIER
Antibodies		
Rabbit polyclonal anti-TH	Millipore	Cat#AB152; RRID:AB_390204
Mouse monoclonal anti-CGRP	Rockland	Cat#200-301-D15; RRID:AB_11181162
Rabbit anti-PV	Swant	Cat#PV27; RRID:AB_2631173
Isolectin GS-B4-biotin XX-conjugate	Invitrogen	Cat#I21414
Rabbit monoclonal anti-desmin	Abcam	Cat#Ab32362; RRID:AB_731901
Mouse anti-aSMA (1A4) eFluor 570	eBioscience	Cat#53-9760-82; RRID:AB_2574461
Mouse anti-α-SMA (1A4) eFluor 660	eBioscience	Cat#50-9760-82; RRID:AB_2574362
Bacterial and virus strains		
Virus: PHP.S AAV variant with a Th minimal promoter and Cre	This paper	N/A
Virus: Cre-dependent AAV-hSyn-DIO-hM4D(Gi)-mCherry	This paper	N/A
Chemicals, peptides, and recombinant proteins		
Tamoxifen	Sigma Aldrich	Cat#T5648
4-hydroxytamoxifen	Sigma Aldrich	Cat#H7904
Evan's Blue	Sigma Aldrich	Cat#E2129
CNO	Tocris	Cat#4936
L-norepinephrine hydrochloride	Sigma Aldrich	Cat#74480
compound 21 dihydrochloride, C21	Hello Bio	Cat#HB6124
propranolol hydrochloride	Sigma Aldrich	Cat#P0884
diphtheria toxin, DTX	Sigma Aldrich	Cat#D0564
Fluorescein isothiocyanate–dextran	Sigma Aldrich	Cat#FD2000S
Experimental models: Organisms/strains		
Mouse: $TrkC^{CreERT2}$	This paper	N/A
Mouse: $Avil^{hM3Dq}$	Dhandapani et al., 2018	N/A
Mouse: $TrkC^{CreERT2}$::$Avil^{hM3Dq}$	This paper	N/A
Mouse: $Rosa26^{ChR2\text{-}YFP}$	The Jackson Laboratory	#024109
Mouse: $TrkC^{CreERT2}$::$Rosa26^{ChR2\text{-}YFP}$	This paper	N/A
Mouse: $Avil^{iDTR}$	Stantcheva et al., 2016. EMMA Mouse Repository	EM:10409
Mouse: $TrkC^{CreERT2}$::$Avil^{iDTR}$	This paper	N/A
Mouse: $TrkC^{CreERT2}$::$Avil^{iDTR}$::$Rosa26^{ChR2\text{-}YFP}$	This paper	N/A
Mouse: $Th^{tm1(cre/Esr1)Nat}$	The Jackson Laboratory	#008532
Recombinant DNA		
BAC containing *TrkC* mouse locus	SourceBioscience	#RP23-38E14
modified CreERT2-pA-Frt-Ampicillin-Frt cassette	This paper	N/A
Minimal Th promoter	Liu et al., 1997. Addgene	#80336
Software and algorithms		
Patchmaster	HEKA	https://www.heka.com/downloads/downloads_main.html#down_patchmaster_next
LabChart 4	ADInstruments	https://www.adinstruments.com/support/software
gHRV 1.6	Rodríguez-Liñares et al., 2014	https://ghrv.software.informer.com/1.6/
ImageJ	Schneider et al., 2012	https://imagej.nih.gov/ij/download.html

RESOURSE AVAILABILITY

Lead contact

Further information and requests for resources, reagents and mouse lines should be directed to the lead contact Paul Heppenstall (paul.heppenstall@embl.it).

Material availability

All reagents generated in this study are available from the lead contact with a completed Materials Transfer Agreement.

Data and code availability

The datasets supporting the current study have not been deposited in a public repository but are available from the corresponding author on request.

EXPERIMENTAL MODEL AND SUBJECT DETAILS

Transgenic animals

Generation of TrkC^{CreERT2} mice

A bacterial artificial chromosome (BAC) containing the *TrkC* mouse locus was obtained from SourceBioscience (RP23-38E14) and a modified CreERT2-pA-Frt-Ampicillin-Frt cassette was inserted into the ATG of *TrkC*. The positive clones were confirmed by PCR and a full-length sequencing of the inserted cassette was performed. The ampicillin cassette was then removed using bacterial Flp and the accomplished removal was confirmed by sequencing analysis. Purified BAC DNA was then dissolved into endotoxin-free TE and prepared for intracytoplasmic sperm injection (ICSI). The method successfully produced offspring and the mice genotype was determined by performing PCR using the following primers: gcactgatttcgaccaggtt (fwd) and gagtcatccttagcgccgta (rev), yielding products of 408 bp.

Avil^{hM3Dq} mice

For gain of function studies, Avil^{hM3Dq} mice as described previously (Dhandapani et al., 2018) were crossed to TrkC^{CreERT2} to generate TrkC^{CreERT2}::Avil^{hM3Dq} heterozygous mice.

Rosa26$^{ChR2\text{-}YFP}$ mice

For optogenetic experiments, TrkC^{CreERT2} mice were crossed to Rosa26$^{ChR2\text{-}YFP}$ mice (The Jackson Laboratory, 024109) to generate TrkC^{CreERT2}::Rosa26$^{ChR2\text{-}YFP}$ mouse line.

Avil^{iDTR} mice

For diphtheria toxin-mediated ablation, Avil^{iDTR} mice, as described in Stantcheva et al. (2016), were crossed to TrkC^{CreERT2} to generate TrkC^{CreERT2}::Avil^{iDTR} heterozygous mice. Triple transgenic mice were also generated by crossing TrkC^{CreERT2}::Avil^{iDTR} to Rosa26$^{ChR2\text{-}YFP}$ mice. The obtained TrkC^{CreERT2}::Avil^{iDTR}::Rosa26$^{ChR2\text{-}YFP}$ mice were used as a reporter line in ablation experiments. For all the experiments, littermates lacking Cre were used as controls.

Male mice, 8-10 weeks old were used in experiments. All mice were were housed in the EMBL Epigenetics and Neurobiology Unit, Rome, according to the Italian legislation (Art. 9, 27 Jan 1992, no 116) under license from the Italian Ministry of Health and in compliance with the ARRIVE guidelines. Experimental protocols were approved by the EMBL Rome Ethics Committee and the Italian Ministry of Health.

Attempts to genetically isolate TrkC^{+}/Th^{+} neurons

In order to genetically isolate TrkC^{+}/Th^{+} neurons we tried two different intersectional approaches using either a transgenic mouse line or AAV delivery of a transgene. For the transgenic mouse approach we obtained a previously described Th-IRES-CreER line (*Th$^{tm1(cre/Esr1)Nat}$*, 008532 from JAX) and initially assessed recombination efficiency in the peripheral nervous system. We crossed the line with a Rosa26$^{ChR2\text{-}YFP}$ reporter but were unable to detect reporter signal in either skin or DRG. We further bred the line to homozygosity, and used antibodies against YFP to increase detection sensitivity, but again, were not able to observe any recombination in peripheral neurons. Of note this strain is different from that used to previously characterize Th positive DRG neurons (Li et al., 2011), which at the time was not available.

We thus turned to an AAV delivery approach using a minimal Th-promoter (Liu et al., 1997) to drive Cre (Gompf et al., 2015). We generated a PHP.S AAV variant with a Th minimal promoter and Cre, and applied it to dissociated DRG neurons from Rosa26$^{ChR2\text{-}YFP}$ mice. We observed strong YFP fluorescence, however upon staining cultures with a Th antibody, we detected minimal overlap of Th immunoreactivity with the Th minimal promoter driven expression.

METHOD DETAILS

Tamoxifen treatment

To induce the expression of Cre, adult mice (older than 8 weeks of age) were treated intraperitoneally (i.p.) with 75 mg/kg of body weight of tamoxifen (Sigma Aldrich, T5648) dissolved in sunflower seed oil (Sigma Aldrich, S5007) for 3 consecutive days. Mice were then used for experiments at least one week after the last injection.

In some cases, to restrict the expression of Cre to DRG neurons, TrkC^{CreERT2}::Rosa26$^{ChR2\text{-}YFP}$ mice were treated with a single intrathecal (i.t.) injection of 45 ng of 4-hydroxytamoxifen (4-OH Tamoxifen, Sigma Aldrich, H7904). Experiments were performed at least one week after the treatment.

Electrophysiology

Whole cell patch clamp recordings from dissociated small TrkC$^+$ DRG neurons were acquired with an EPC-10 double patch clamp amplifier (HEKA) controlled with Patchmaster© software (HEKA). Patch pipettes with a tip resistance of 2-5 MΩ were filled with intracellular solution 110 mM KCl, 10 mM NaCl, 1 mM MgCl2, 1 mM EGTA, 10 mM HEPES, 2 mM guanosine 5′-triphosphate (GTP) and 2 mM adenosine 5′-triphosphate (ATP) adjusted to pH 7.3 with KOH. The extracellular solution (ECS) contained 140 mM NaCl, 4 mM KCl, 2 mM CaCl2, 1 mM MgCl2, 4 mM glucose, 10 mM HEPES, adjusted to pH 7.4 with NaOH. Cells were clamped to a holding potential of −60 mV. Pipette and membrane capacitance were compensated using the auto function and series resistance was compensated to a 50%. For capsaicin and pH stimulation, clamped cells were perfused for 20 s with ECS with 1 μM Capsaicin (Sigma) or ECS adjusted to pH 5.4. For mechanical stimulation, a series of mechanical stimuli in 1 μm increments with a fire-polished glass pipette (tip diameter 2-3 μm) were applied at an angle of 45° and with a velocity of 1 μm/ms by a piezo driven micromanipulator (Nanomotor© MM3A, Kleindiek Nanotechnik). The evoked whole cell currents were recorded with a sampling frequency of 10 kHz and filter with 2.9 kHz low-pass filter. The mechanically activated currents were classified according to the inactivation kinetics obtained by fitting the current decay to a single exponential curve ($C1+C2*\exp(-(t-t0)/\tau)$) in rapidly adapting (RA, tau < 10 ms) and intermediate adapting (IA, tau 15-30 ms). No slowly adapting currents (200-300 ms) were observed in the small TrkC$^+$ population. For the classification of pH elicited currents, the inactivation kinetic was also calculated by fitting the current decay to a single exponential curve.

Immunofluorescence

Ganglia were dissected and fixed in 4% PFA overnight at 4°C. They were then embedded in 2% agarose (Sigma Aldrich, A9539) and cut in 50 μm sections using a vibratome (Leica, VT1000S). After an incubation of 30 minutes with a blocking solution containing 5% goat serum and 0.01% Tween-20 in PBS, the sections were incubated with one or more primary antibodies in blocking solution overnight at 4°C. As a negative control, sections were incubated without primary antibodies. The next morning, secondary antibodies in blocking solution were added and the sections were incubated for 1 hour and 30 minutes at room temperature (RT). After two washes with PBS, slides were mounted with prolong gold (Invitrogen, P36930).

To examine TrkC$^+$ peripheral afferents, mice were injected intravenously (i.v.) with a solution of 2% Evan's Blue (Sigma Aldrich, E2129) in PBS. After 30 minutes, the skin was carefully dissected and fixed in 4% PFA overnight at 4°C. After permeabilizing with PBS-T (0.3% TritonX in PBS) for 30 minutes at RT, the tissue was incubated in a blocking solution (10% goat serum in PBS-T) for 2 hours at RT and then with one or more primary antibodies (Table 1) in blocking solution overnight at 4°C. Secondary antibodies were added in blocking solution for 1 hour and 30 minutes at RT and then the tissue was whole-mounted using prolong gold.

For immunofluorescence experiments, the following primary antibodies and lectins were used: Rabbit anti-TH (1:1000) Millipore, AB152; Mouse anti-CGRP (1:500) Rockland, 200-301-D15; Rabbit anti-PV (1:1000) Swant, PV27; Isolectin GS-B4-biotin XX-conjugate (1:100) Invitrogen, I21414; Rabbit anti-desmin (1:200) Abcam, Ab32362; Mouse anti-αSMA (1A4) eFluor 570 (1:500), eBioscience, 53-9760-82; Mouse anti-α-SMA (1A4) eFluor 660 (1:500) eBioscience, 50-9760-82.

All secondary antibodies were Alexa-conjugated and were used at a concentration of 1:1000. Streptavidin-conjugated secondary antibodies were used at a concentration of 1:500.

All images were acquired using a Leica SP5 confocal microscope and analyzed using ImageJ.

Ex-vivo live imaging

Mice were injected i.v. with a solution of 2% Evan's Blue. After 30 minutes, the skin of the hind limb was carefully dissected and placed in a bath chamber where physiological conditions were maintained (32°C, 5% CO_2, synthetic interstitial fluid: 108 mM NaCl, 3.5 mM KCl, 0.7 mM $MgSO_4$, 26 mM $NaHCO_3$, 1.7 mM NaH_2PO_4, 1.5 mM $Cacl_2$, 9.5 mM sodium gluconate, 5.5 mM glucose and 7.5 mM sucrose at a pH of 7.4).

In the case of TrkC^{CreERT2}::Avil^{hM3Dq} mice, 50 μM of Clozapine-N-oxide (CNO, Tocris, 4936) was added to the chamber. As a positive control, L-norepinephrine hydrochloride (Sigma Aldrich, 74480) was used at a concentration of 10 mM.

For TrkC^{CreERT2}::Rosa26$^{ChR2\text{-}YFP}$ mice, the skin was stimulated for 40 s every minute for 14 minutes with a built-in 488 nm microscope laser.

All tissues were imaged using a Nikon Ti Eclipse spinning disk confocal microscope. Images were acquired every minute for 14 minutes and analyzed using ImageJ. For each blood vessel, the change in diameter was measured by randomly selecting three areas

and comparing the initial diameter with the diameter at the end of the acquisition. The mean diameter change for each vessel was then expressed as percentage of the initial diameter.

Administration of DREADD ligands

In order to systemically activate TrkC^{+} neurons, TrkC^{CreERT2}::Avil^{hM3Dq} mice were injected i.p. with 2.5 mg/kg of body weight of the DREADD agonist compound 21 dihydrochloride (C21, Hello Bio, HB6124).

For local activation or silencing, 2.5 mg/kg of CNO was injected subcutaneously in the hind paw of TrkC^{CreERT2}::Avil^{hM3Dq} mice and TrkC^{CreERT2} injected with Cre-dependent AAV-hSyn-DIO-hM4D(Gi)-mCherry, respectively.

Propranolol administration

The nonselective β-adrenergic blocker propranolol hydrochloride (Sigma Aldrich, P0884) was injected i.p. at a concentration of 5 mg/kg of body weight. The injection was performed immediately after the administration of the DREADD ligand.

Diphtheria toxin injection

TrkC^{CreERT2}::Avil^{iDTR} mice were injected i.p. with 40 ng/g of body weight of diphtheria toxin (DTX, Sigma Aldrich, D0564) as has been described previously and shown to be selective and effective (Abrahamsen et al., 2008; Arcourt et al., 2017; Breitman et al., 1987; Buch et al., 2005; Cavanaugh et al., 2009; Dhandapani et al., 2018; Palmiter et al., 1987; Stantcheva et al., 2016). All mice were monitored during the injection period and blood pressure, heart rate and blood flow were measured before the injection of DTX and 16, 24 and 32 hours after.

Blood pressure measurements

Mice were anesthetized with a 2% isoflurane and medical air mixture through a nose cone and placed on a heat pad at 37°C. Blood pressure (BP) was measured using a Non-Invasive Blood Pressure (NIBP) system (AD Instruments) paired with a PowerLab 4/20 ML840 (AD Instruments) and LabChart 4 software to acquire and analyze data. For each measurement, BP was registered four times per mouse with a 1-minute interval and the mean value was recorded.

Heart rate measurements

Mice were anesthetized with 2% isoflurane and kept at 37°C using a heat pad. The heart rate was monitored for 30 or 60 minutes using a PhysioSuite MouseSTAT (Kent Scientific) and Free Serial Port Terminal 1.0.0.710 software. All data were analyzed using gHRV 1.6 software (Rodríguez-Liñares et al., 2014).

Laser speckle contrast imaging

To analyze blood flow, recordings were performed using a 780 nm, 100mW laser (LaserLands) at a working distance of 5 cm and a Leica Z16 Apo microscope with a high resolution camera (AxioCam MRM, Carl Zeiss) with 5 ms exposure time at maximum speed for 100 cycles. Data were then analyzed using a custom MATLAB script (Gnyawali et al., 2017), and vascularized area analyzed using ImageJ (mm^2 occupied by blood vessels in the field of view at each time point).

For gain of function experiments, mice were anesthetized with an i.p. injection of 90 mg/kg ketamine (Lobotor, Acme) and 0.5 mg/kg medetomidine (Domitor, Orion Pharma) and their hind paw was attached using double-sided tape to a plastic platform. Images were acquired before the treatment with CNO and after its administration every 2 minutes for 30 minutes.

For ablation experiments, mice were anesthetized with 2% isoflurane and their ear was attached to a plastic platform with the external side up, facing the camera. Images were acquired before the injection of DTX and 16, 24 and 32 hours after.

In-vivo three-photon (3P) imaging

To analyze blood flow and blood vessel cross-section changes *in-vivo*, we performed 3P microscopy using a custom-built system. 3P-excitation of fluorescein labeled blood plasma was done at 1300nm by using a non-collinear optical parametric amplifier (NOPA, Spectra Physics) pumped by a regenerative amplifier (Spirit, Spectra Physics) with a repetition rate of 400kHz. Dispersion compensation to maintain short pulse durations (50 fs) at the sample plane was achieved with a custom-built dispersion compensation unit (Kong and Cui, 2013). For imaging the power under the objective lens (Olympus 25x, 1.05NA, XLPLN25XWMP2) ranged from 8mW to 12mW.

To label blood vessels *in-vivo,* mice were injected with 150μl of 5% w/v fluorescein-dextran (Sigma FD2000S 2MDa). For experiments mice were anesthetized with 2% isoflurane and the hair of the ear was removed using hair removal crème. The ear was attached to a cover glass using double sided tape with the external side facing the objective lens.

For optogenetic stimulation, an area of the ear of TrkC^{CreERT2}::Rosa26$^{ChR2\text{-}YFP}$ or control mice with a diameter of 2mm was illuminated with a 470nm LED (Thorlabs M470L4) for 1min. Stimulation consisted of 10ms bursts at 5Hz with 3mW/mm^2 excitation power.

For volume/stack data analysis, first a median filter (3x3 kernal; ImageJ) was applied before manual segmentation of the blood vessel. A maximum intensity image was generated from the segmented stack and the cross-sectional area of the blood vessel was measured using the 'analyze particles' plugin from ImageJ. For visualization purposes of the orthogonal views the image stack was interpolated in the axial dimensions by a factor 5.

In general, 3P imaging data was acquired at 0.69Hz, and typically 20 frames were averaged to improve signal-to-noise, manually segmented and the area analyzed using the 'analyze particles' plugin from ImageJ.

Behavioral testing

All behavior experiments were performed on adult male mice (> 8 weeks of age). Littermates not expressing Cre were used as controls. The experimenter was always blind to the genotype of the mice. Unless otherwise specified, all tests were performed 1 hour after local injection of CNO.

Acetone drop test

Mice were habituated on an elevated platform with a mesh floor for 30 minutes. A single drop of acetone was sprayed on the hind paw with a blunt syringe making sure not to touch the paw. The test was repeated 5 times per mouse and the behavioral responses were scored as follows:

0 = no response
1 = paw withdrawal or single flick
2 = repeated flicking
3 = licking of the paw

Paintbrush test

After a habituation time of 30 minutes on an elevated platform with a mesh floor, the hind paw of mice was stimulated with a paintbrush in the heel-to-toe direction. The responses were scored according to Duan et al. (2014):

0 = no response
1 = paw withdrawal
2 = flicking of the paw
3 = licking of the paw

Von Frey test

Mice were placed on an elevated platform with a mesh floor and habituated for 30 minutes. The hind paw was stimulated with calibrated von Frey filaments (North coast medical, NC12775-99) and the 50% withdrawal thresholds were calculated using the Up-Down method previously described (Chaplan et al., 1994).

To measure the sensitivity to mechanical pain over time, the hind paw of $TrkC^{CreERT2}$::$Avil^{hM3Dq}$ mice was stimulated with a 0.02 g filament five times, 10 minutes, 25 minutes and 40 minutes after the local injection of CNO. The percentage of withdrawals was calculated per each time point.

Hot plate test

To measure thermal nociception over time, mice were placed on top of a hot plate (Ugo Basile, 35150) set at 52°C and the latency to response, indicated as flicking or licking of the hind paw, was measured before local injection of CNO in the hind paw and 10, 25 and 40 minutes after.

QUANTIFICATION AND STATISTICAL ANALYSIS

All statistical data are represented as standard error of the mean (SEM). Student's t test and/or 2-way repeated-measures ANOVA were used and $p < 0.05$ was considered statistically significant.

Cell Reports, Volume *35*

Supplemental information

Identification of a population of peripheral sensory neurons that regulates blood pressure

Chiara Morelli, Laura Castaldi, Sam J. Brown, Lina L. Streich, Alexander Websdale, Francisco J. Taberner, Blanka Cerreti, Alessandro Barenghi, Kevin M. Blum, Julie Sawitzke, Tessa Frank, Laura K. Steffens, Balint Doleschall, Joana Serrao, Denise Ferrarini, Stefan G. Lechner, Robert Prevedel, and Paul A. Heppenstall

Supplemental Information

This file includes:

Supplemental Figures S1 to S7

Other Supplemental Materials for this manuscript include the following:

Videos S1 to S7

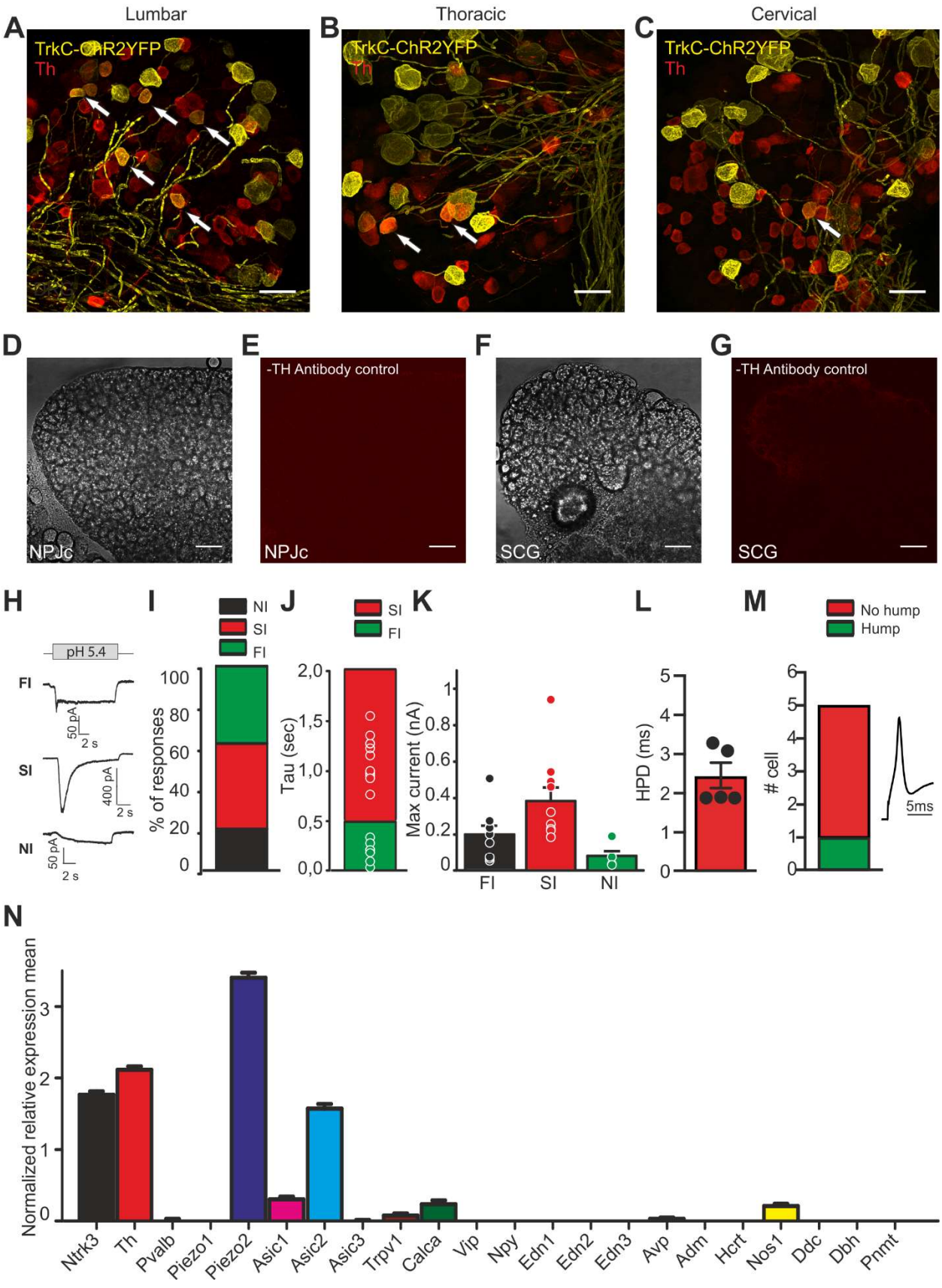
A
Lumbar
TrkC-ChR2YFP
Th
B
Thoracic
TrkC-ChR2YFP
Th
C
Cervical
TrkC-ChR2YFP
Th
D
NPJc
E
-TH Antibody control
NPJc
F
SCG
G
-TH Antibody control
SCG
H
pH 5.4
FI
50 pA
2 s
SI
400 pA
2 s
NI
50 pA
2 s
I
NI
SI
FI
% of responses
J
SI
FI
Tau (sec)
K
Max current (nA)
FI
SI
NI
L
HPD (ms)
M
No hump
Hump
cell
5ms
N
Normalized relative expression mean
Ntrk3
Th
Pvalb
Piezo1
Piezo2
Asic1
Asic2
Asic3
Trpv1
Calca
Vip
Npy
Edn1
Edn2
Edn3
Avp
Adm
Hcrt
Nos1
Ddc
Dbh
Pnmt

Figure S1. Characterization of TrkC^{+} neurons. Related to Figure 1

(A-C) Immunofluorescent staining of DRG sections from TrkC^{CreERT2}::Rosa26$^{ChR2\text{-}YFP}$ mice labelled with anti-Th antibodies. TrkC expression was investigated in lumbar DRG (A), thoracic DRG (B) and cervical DRG (C). Double positive neurons are indicated by arrows. Scale bars, 50 µm. (D-G) Antibody controls for Th showing phase contrast (D and F) and red channel images(E and G) in the NPJc and SCG. (H) Example traces of pH activated currents recorded in small TrkC^{+} neurons (24 cells from 3 mice). (I) Distribution of neurons according to the pH current type: fast inactivating (FI), slowly inactivating (SI) and non-inactivating (NI). (J) Distribution of the inactivation constants of the pH elicited currents. (K) Comparison of the maximal current amplitude in the different pH elicited current types. (L) Action potential Half Peak Duration (HPD) in small TrkC^{+} neurons (n=5). (M) Proportion of TrkC^{+} neurons with a hump on the falling phase of the action potential (left) and action potential example (right). (N) Gene expression panel of TrkC^{+} Th^{+} positive neurons (n=197) (data taken from (Zeisel et al., 2018)).

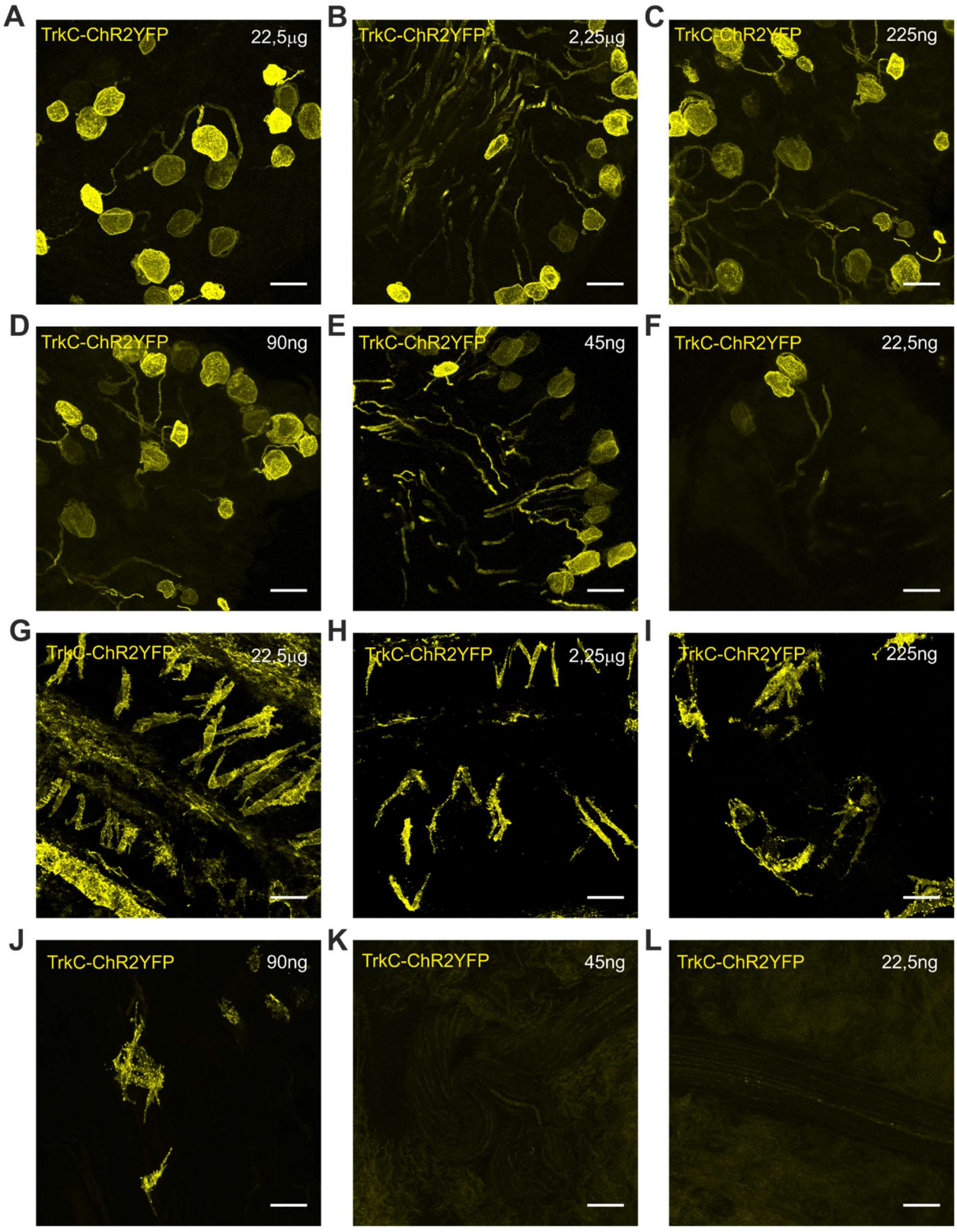
A
TrkC-ChR2YFP
22,5µg
B
TrkC-ChR2YFP
2,25µg
C
TrkC-ChR2YFP
225ng
D
TrkC-ChR2YFP
90ng
E
TrkC-ChR2YFP
45ng
F
TrkC-ChR2YFP
22,5ng
G
TrkC-ChR2YFP
22,5µg
H
TrkC-ChR2YFP
2,25µg
I
TrkC-ChR2YFP
225ng
J
TrkC-ChR2YFP
90ng
K
TrkC-ChR2YFP
45ng
L
TrkC-ChR2YFP
22,5ng

Figure S2. Concentration dependent recombination upon intrathecal injection of 4-OH tamoxifen. Related to Figure 2.

(A-F) Cre-driven recombination and YFP expression in DRG neurons and vSMC. (G-L) At lower concentrations, YFP is evident only in DRG and not in vSMC. Scale bars 50 μm.

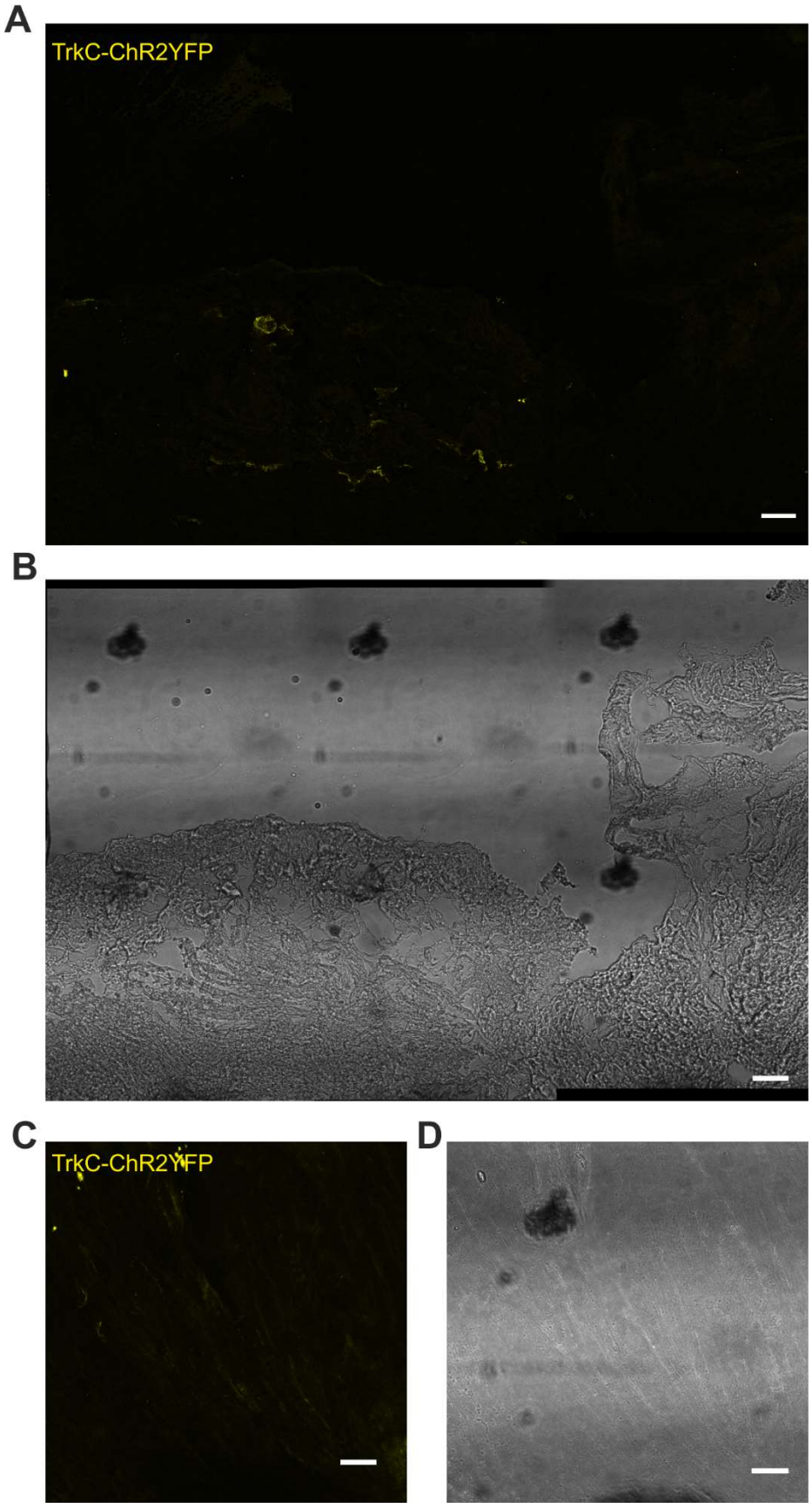
A
TrkC-ChR2YFP
B
C
TrkC-ChR2YFP
D

Figure S3. TrKC^{CreERT2} mediated recombination in the heart. Related to Figure 2.

(A and B) Large scale mosaic image of a section of heart tissue from TrkC^{CreERT2}::Rosa26$^{ChR2\text{-}YFP}$ mice. (A) YFP channel, (B) phase contrast. (C and D) Higher magnification image from the ventricles. (C) YFP channel, (D), phase contrast. Note the absence of TrkC+ neurons. Scale bars 50µm.

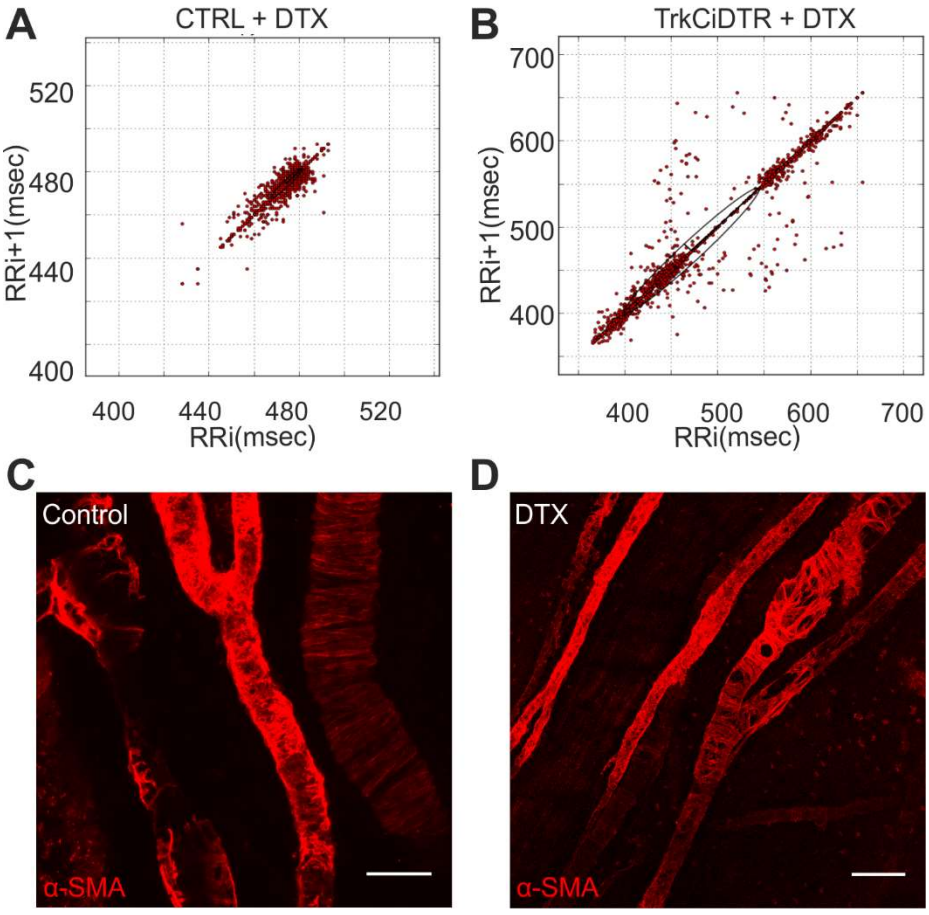

Figure S4. Ablation of TrkC^{+} neurons. Related to Figure 4.

(A and B) Representative Poincaré plots of a control (A) and TrkC^{CreERT2}::Avil^{iDTR} (B) mouse treated with DTX. (C and D) Representative images of vSMC labelled with an α-SMA antibody in control (C) and TrkC^{CreERT2}::Avil^{iDTR} (D) mouse treated with DTX.

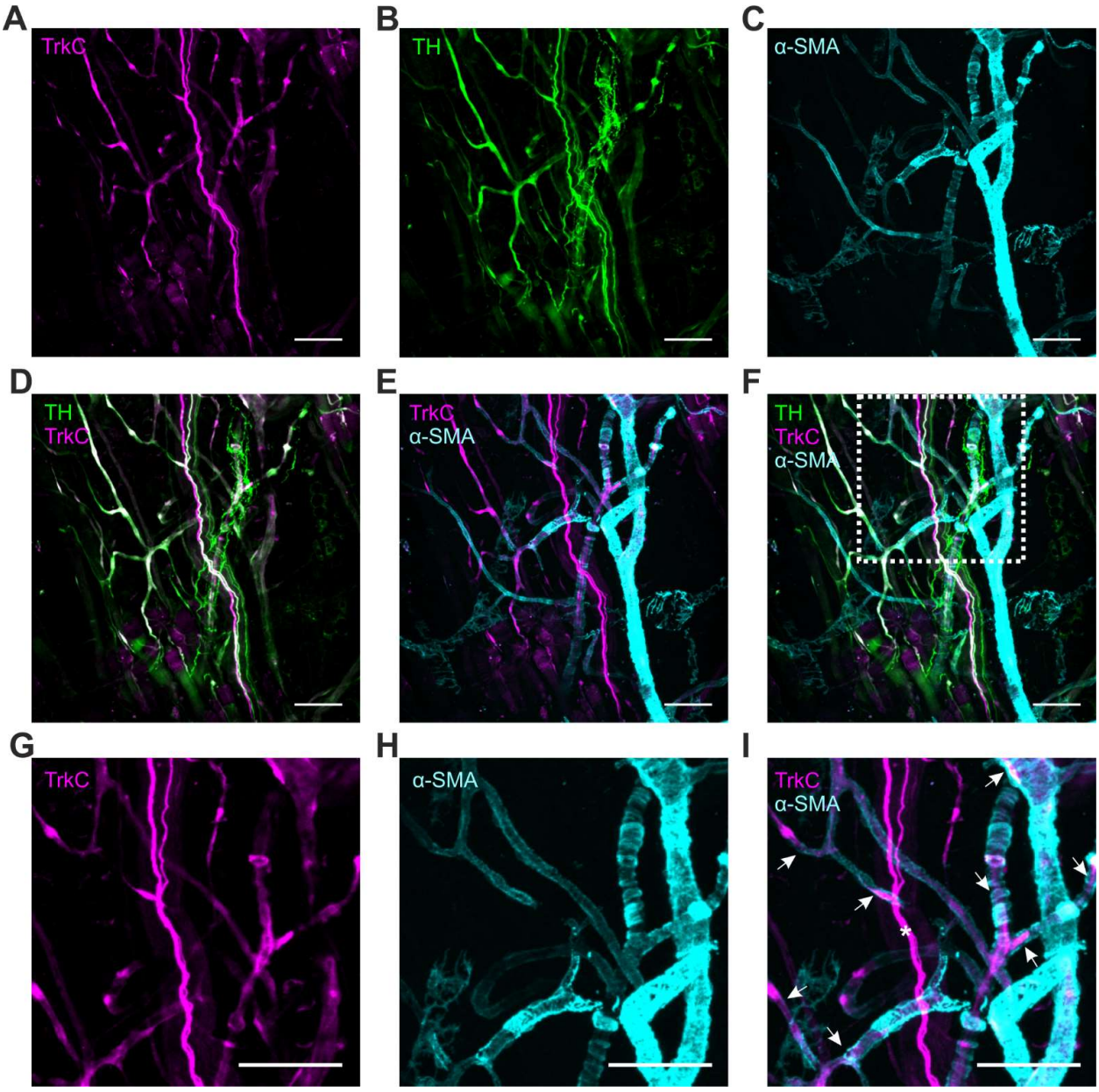

Figure S5. Imaging of TrkC$^+$ neurons in whole mount ear preparations. Related to Figure 5.
(A and F) Representative low magnification images of TrkC$^+$ neurons in whole mount ear preparations. (A) TrkC$^+$ neurons (magenta). (B) TH$^+$ neurons (green). (C) α-SMA labelled vSMC (cyan). (D) TrkC$^+$ neurons coexpress TH$^+$ (E) TrkC$^+$ neurons were often closely associated α-SMA labelled vSMC. (F) Composite image of TrkC, TH and α-SMA labelling. (G-I) High magnification images of area indicated by dotted box in (F). (G) TrkC$^+$ neurons. (H) α-SMA labelled vSMC. (I) Association of TrkC$^+$ neurons with blood vessels (arrows). The larger TrkC$^+$ fiber which runs vertically through the center of the image is part of a nerve fascicle (asterisk). All scale bars 100μm.

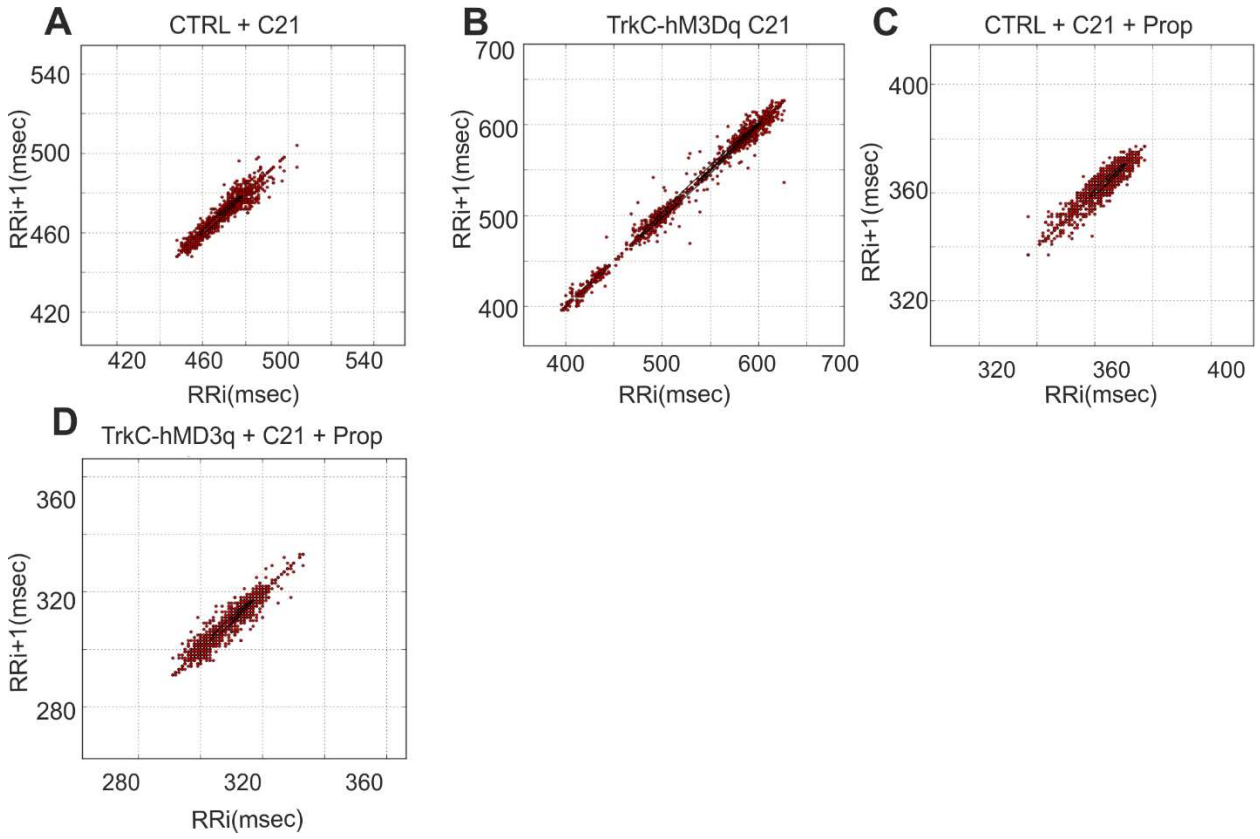

Figure S6. Activation of TrkC^{+} neurons. Related to Figure 6.
(A and B) Poincaré plot of a control (A) and a TrkC^{CreERT2}::Avil^{hM3Dq} (B) mouse treated with C21. (C and D) Representative Poincaré plot of a control mouse treated with C21 and Propranolol (C) and a TrkC^{CreERT2}::Avil^{hM3Dq} mouse treated with C21 and Propranolol (D).

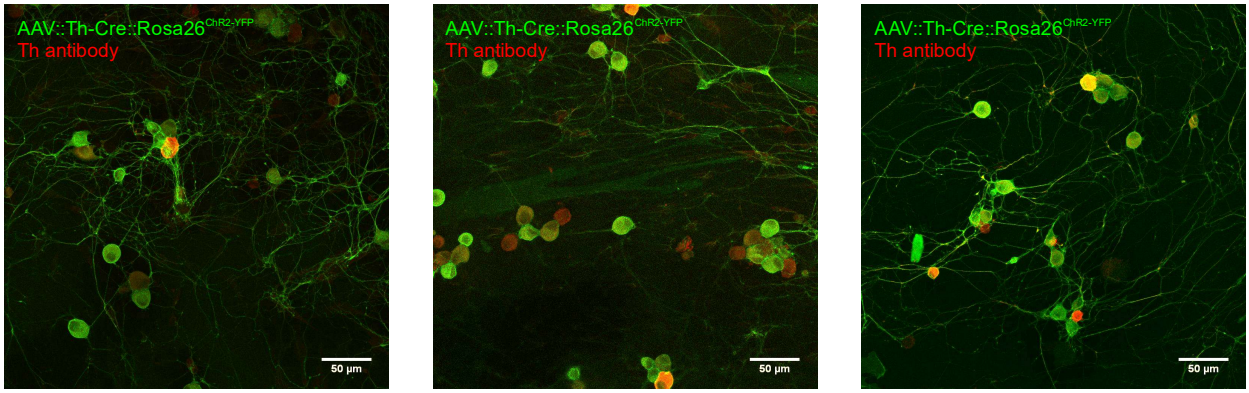

Figure S7. PHP.S AAV Th promoter driven Cre recombination. Related to STAR Methods.
Examples of Th promoter driven Cre recombination and Th antibody staining in DRG neurons